Geothermics 115 (2023) 102826

Contents lists available at ScienceDirect

Geothermics

journal homepage: www.elsevier.com/locate/geothermics

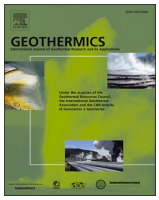

Geochemical behaviors of rare earth elements in granite-hosted geothermal systems in SE China

Fen Zhang [a,b], Yiman Li [a,b,*], Xiaocheng Zhou [c,*], Tianming Huang [a,b], Jiao Tian [c], Yuanzhi Cheng [a,b], Yajing Zhao [a,b]

[a] Key Laboratory of Shale Gas and Geoengineering, Institute of Geology and Geophysics, Chinese Academy of Sciences, Beijing 100029, China
[b] College of Earth and Planetary Sciences, University of Chinese Academy of Sciences, Beijing 100049, China
[c] Institute of Earthquake Forecasting, China Earthquake Administration, Beijing 100036, China

ARTICLE INFO

Keywords:
Geothermal systems, REEs
Seawater mixing effect
Salinity mutation
REEs speciation

ABSTRACT

Rare earth elements (REEs) are effective indicators in tracking water-rock interactions in the hydrothermal systems. Subject to multiple environmental effects, none a unified conclusion has been achieved to generalize the mechanism of diversifying the REEs in various thermal systems. Low-medium temperature hydrothermal systems occurring in fractured-granite exist widely in South China. However, geochemical behavior of REEs in geothermal water is not well studied though there are lots of REEs deposits. This study focuses on hydrogeochemical characteristics of REEs and constrains from salinity. Results show that the TDS (total dissolved solids) mutation due to transfer of sedimentary environments from coastal to relatively inland areas caused the great differentiation of REEs and their species. When TDS is greater than 1 g/L, Ln^{3+}, $LnOH^{2+}$, $LnSO_4^+$, and LnF^{2+} (Ln represents REEs) prevail and fractions of them except $LnOH^{2+}$ are positively correlated with TDS. In contrast, when TDS is less than 1 g/L, $LnCO_3^+$ and Ln $(CO_3)_2^-$ constitute the most important part and mutually compete in fluids. A positive Eu anomaly is proved to originate primarily from the preferential dissolution of Eu-rich minerals and the seawater intrusion somewhat contributed to the negative Ce anomaly. This work first proposed the salinity effect on REEs by analysis of the *in-situ* sampling thermal waters that may have been neglected before and provided a new perspective to comprehensively understand the occurrence and migration mechanisms of REEs in different hydrothermal systems.

1. Introduction

Rare earth elements (REEs) comprise the lanthanide elements (La-Lu) and the element Y (Number 39) in the periodic table. Generally, they are incorporated into a special geochemical element group with particularly coherent chemical properties and tend to move integrally in the course of the earth's evolution (de Baar et al., 1988; McLennan, 2018). Nevertheless, subtle variations in the properties of this group allow their fractionation to sensitively capture ample information about geological and geochemical processes (Hetherington et al., 2010; Muzaffer Karadağ et al., 2009; Murray et al., 1990). The state-of-the-art testing technology for REEs makes it widely be used to constrain processes involved in magmatism and metamorphism characterization (He et al., 2021), mantle and crustal evolution (Gleason et al., 2000; Motoki et al., 2015), nuclear waste contamination tracking (Ménard et al., 1998; Wood, 1990), restoring of the protolith of the metamorphic rocks (Li et al., 2013), and deciphering of the weathering process and water-rock interactions (Cholet et al., 2019; Esmaeili-Vardanjani et al., 2013). Recognized as a powerful tracer in tracking chemical processes in aqueous systems, currently REEs are fast becoming a key instrument in hydrogeochemistry research (Banner et al., 1989; Fee et al., 1992; Gosselin et al., 1992; Verplanck et al., 2004).

Laveuf and Cornu (2009) reviewed and reported that the concentration of REEs is usually quite low in groundwater, and it is 1.1∼1196 $ng{\cdot}L^{-1}$ with an average value of 57.2 $ng{\cdot}L^{-1}$. Accordingly, when REEs enter the groundwater system, minor changes in the complex underground environment and possible hydrochemical effects, including chemical weathering, dissolution and precipitation, adsorption and desorption, and redox reactions, may imprint more intensely on REEs than any other element in groundwaters, which creates great superiorities for REEs to address groundwater-pertinent issues (Bwire Ojiambo et al., 2003; Noack et al., 2014; Smedley, 1991). REEs in groundwaters

* Corresponding authors.
E-mail addresses: liyiman@mail.iggcas.ac.cn (Y. Li), zhouxiaocheng188@163.com (X. Zhou).

https://doi.org/10.1016/j.geothermics.2023.102826
Received 7 January 2023; Received in revised form 22 August 2023; Accepted 4 September 2023

are confirmed to be derived chiefly from surrounding rocks through which they flow (Johannesson et al., 1997) and thus thought to be useful for examining the water-rock interactions (Bragin et al., 2018; Bulia and Enzweiler, 2018; Oliveri et al., 2019; Smedley, 1991; Xiao et al., 2010). Besides, physicochemical properties of aqueous environments like the pH (Elderfield et al., 1990; Noack et al., 2014), redox conditions (de Baar et al., 1988; Liu et al., 2016), temperature (Bragin et al., 2018; Shakeri et al., 2015) are usually documented to predominate REEs mobility as well. However, controversial interpretations for influential factors of REEs have persisted and no a unified conclusion has been achieved to generalize the mechanism of diversifying REEs in various groundwater systems.

Recently, with the rapid development of the geothermal industry and increasing demands for development and utilization of geothermal energy, REEs have also received a crucial attention to reveal detailed hydrogeochemical processes in geothermal systems by clarifying their migration and transformation in thermal waters in the past few decades (Göb et al., 2013; Shakeri et al., 2015; Wang et al., 2020). Similar to groundwaters, what caused the large discrepancies in REEs for thermal waters in different geothermal systems still remains a subject of debate (Guo and Zhang, 2022; Haas et al., 1995; Hatipoğlu Temizel et al., 2020; Shakeri et al., 2015). Guangdong province, with densely exposed hot springs and widely distributed geothermal wells, has been universally acknowledged as a province with great potential for developing geothermal resources (Lu and Liu, 2015; Wang et al., 2018; Yuan et al., 2013). Making sense of hydrochemical characteristics and complicated water-rock reactions in geothermal water is of great significance for a detailed grasp of local geothermal system evolution. However, previous investigations predominantly focus on the major elements of thermal water and surrounding rocks here (Cao, 2004; Lin et al., 2020; Ling et al., 2006; Yan et al., 2019) and researches on the trace elements especially for REEs are sparse (Li et al., 2022b; Luo et al., 2022; Wu et al., 2003; Yuan et al., 2014). Meanwhile, the special coastal tectonic location makes the hydrochemical properties of geothermal water more complicated affected by seawater mixing (Awaleh et al., 2015; Chen et al., 2016; Wang et al., 2018), all of which requires an all round knowledge of REE geochemistry of thermal waters in offshore areas.

Considering the aforementioned, this study intends to constrain the behavior of geothermal waters by comprehensively characterizing the geochemistry features and potential reactions of the main geothermal fields in Guangdong province based on the analysis of major element and chosen trace element compositions. Moreover, this paper lays particular stress on the distribution and migration of REEs in geothermal waters by content testing and aqueous REEs speciation calculation due to its great sensitivity, and this is possibly expected to contribute to providing some guidance to the development and utilization of geothermal resources (including REEs resources) in coastal regions in the future.

2. Geological settings

The study area is located on the southeastern edge of the Eurasian continent and is a part of the South China Block (SCB), which is affected by the subduction of the Indian Ocean Plate, the Pacific Plate, and the Philippine Sea plate (Wang et al., 2018). The lithology of strata outcropped in different areas in the Guangdong Province is totally different. For the coastal areas of western Guangdong, the strata are relatively well-developed, and the oldest strata can be seen in the Middle-Late Proterozoic, Sinian, and Cambrian strata, in which metamorphic rocks such as schist and gneiss constitute the main types of rocks. Except for metamorphic rocks, the marine sedimentary environment makes sedimentary rocks mainly composed of marine turbidite, clastic rocks, and part of silicon and argillaceous assemblages interspersed with volcanic rocks and carbonate assemblages. In addition, the Cretaceous and Quaternary strata are widely exposed here, and the lithology of the strata mainly includes gravel, sand, silt and clay. Compared with western Guangdong, the outcropping of strata in eastern Guangdong which is closest to the inland areas is relatively newer. The overlying stratum is generally composed of sedimentary rocks and Quaternary sediments with complex sedimentary structures and diverse rock types, such as the gravel layer, the sand layer, silt, and clay. However, for the whole Guangdong Province, the igneous rocks are always the focus of geothermal research. Since the Mesozoic, large-scale intracontinental orogenic belts are developed and magmatic activities frequently occurred, leading to a large area of igneous rocks were formed mainly including granites of the Triassic of the Indosinian phase as well as granites and basalts of the Jurassic and Cretaceous of the Yanshanian phase. Among them, granites constitute the most widely distributed batholith outcrops as igneous rocks in Guangdong province, almost accounting for >40% of the bedrocks (Fig. 1b) (Li et al., 2021; Mao et al., 2018). It is reported that 90% of hot springs in Guangdong Province are located in fault zones within the igneous rock distributed area (Li, 2005). And as the main igneous rock type of geothermal reservoir in the study area, the decay of radioactive elements in granites has been recognized as the primary heat source of geothermal in Guangdong Province (Liao, 2012).

Tectonically, its evolution process is mainly divided into three stages including Plate margin rifting, intra-plate platform, and active continental margin stage with corresponding tectonic movements as the Caledonian (Sinian to Silurian), Indosinian (Devonian to Middle Triassic), and the Yanshan-Himalayan (since Late Triassic), respectively (Huang and Chu, 1995). Long-term tectonic activities have produced a series of magnificently deformed structures, such as large-scale fold belts and deep fault zones (Mao et al., 2015; Wang, 2008). In Guangdong Province, these structures are mostly distributed in NNE or NE-oriented directions chiefly as heat-controlled structures, followed by EW and NW-oriented directions chiefly as heat or water conductive structures. NW-trending faults are grossly formed later, cutting NNE/NE-trending and EW-trending faults (Li, 2005). As shown in Fig. 1c, the predominant fault systems in this region mainly include: Xinyi-Lianjiang, Sihui-Wuchuan, Xinfeng-Enping, Heyuan, Zijin-Boluo, Lianhuashan, Suixi, Gaoyao-Huilai, Fogang-Fengliang, Guidong, and Jiufeng fault zones. (Cai et al., 2002; Lu and Liu, 2015). The existence of these fault structures, accompanied by the uplift of crust and multiple phases of intense magmatic activities, created cardinally favorable conditions for the formation of geothermal resources here (Lu and Liu, 2015; Lin et al., 2020; Wu et al., 2020). Moreover, the vertical high-permeability channel formed by the intersection of faults provides expedient paths for the upwelling of deep geothermal fluids (Zhu, 1982; Geological Survey of Guangdong Province, 1988). This is why most geothermal displays like hot springs in the study area is always at the intersection zones of groups of faults (Li, 2005).

In order to study the hydrochemical genesis of geothermal water and the genetic model of geothermal system evolution in the main geothermal fields in Guangdong Province, from November to December 2020, a total of 77 geothermal water, river water and shallow cold groundwater samples were collected from the Maoming (MM), Xinzhou (XZ), Shenzao (SZ), Huizhou (HZ) and Fengshun (FS) five geothermal fields. Geographically, the MM, XZ, and SZ geothermal fields are obviously closer to the sea than the HZ and FS fields. The sampling points are shown in Fig. 1.

3. Sampling and analysis

A total of 77 samples were collected from December 2019 to November 2021, locations of which were shown in Fig. 1c. Parameters including pH, temperature, electrical conductivity (EC) and oxidation–reduction Potential (ORP) were measured in situ using a potable HACH multi-parameters analyzer (HQ40D). Total alkalinity was also determined on site with the Gran titration method using a HACH Digital Titrator. Sulfide and Fe^{2+} were determined using a portable UV–Visible Spectrophotometer. For SiO_2 analysis, the geothermal water samples

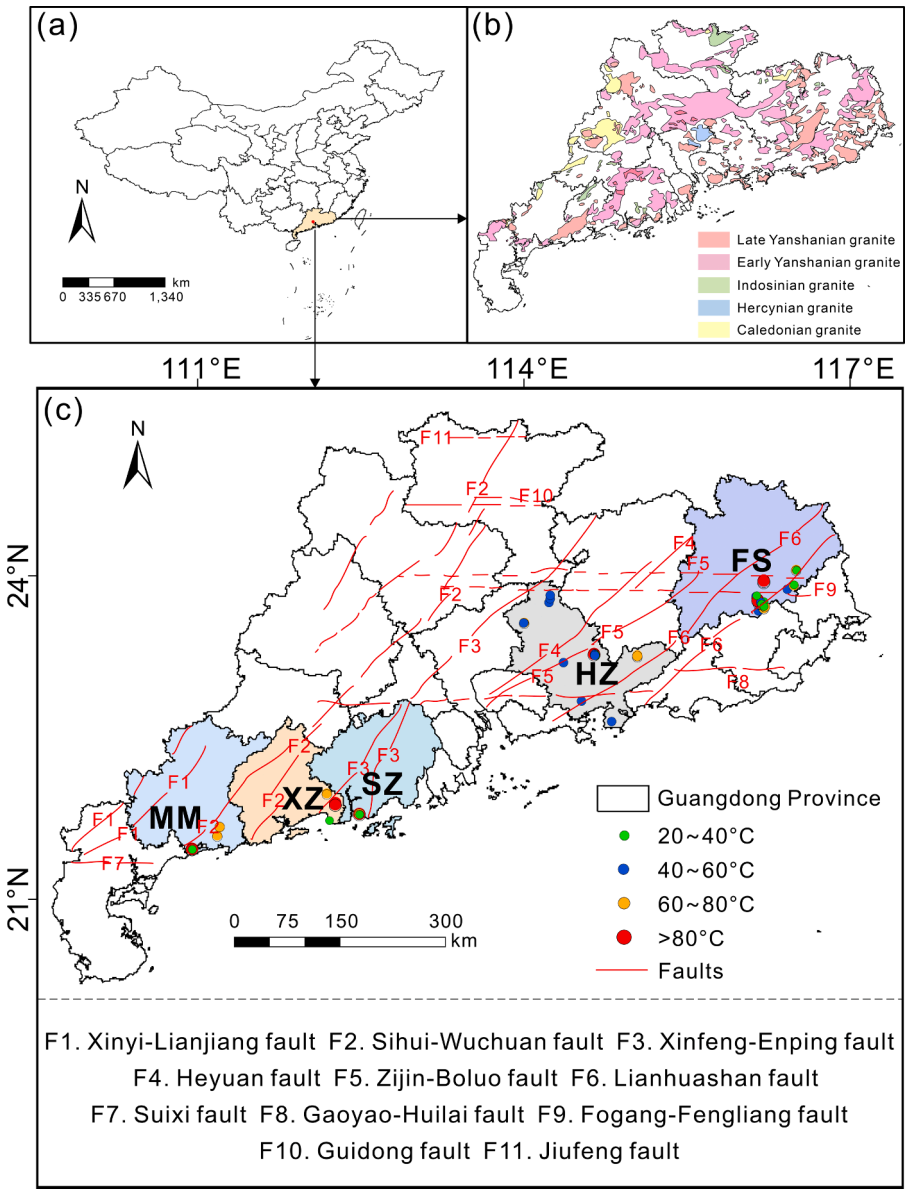

Fig. 1. (a) The geographic location of Guangdong Province. (b) Distribution of granite outcrops in different periods in Guangdong province modified by Li et al. (2021). (c) Sampling locations of the studied geothermal fields. The red lines represent the main faults, in which F1-F6 are mainly distributed along NE/ NNE directions, but F7-F11 mainly along EW directions (modified according to Cai et al., 2002 and Lu and Liu, 2015).

were diluted fivefold using deionized water to prevent polymerization and precipitation. For cation and trace element analysis, ultrapure nitric acid was added to keep the fluid at pH=2. Samples for water chemistry and isotope analysis were filtered through 0.45 μm membranes before bottling in the HDPE bottles. Then, all the water samples were analyzed indoors for major ions and trace elements as well as typical isotopes including $\delta^{18}O_{H2O}$ and $\delta^{2}H_{H2O}$.

Following the field measurements, the collected water samples were guaranteed to be immediately sent to the Beijing Research Institute of Uranium Geology for Si, REEs, and other trace element detection. The analytical methods used were Inductively Coupled Plasma Atomic Emission Spectroscopy (ICP-AES) and Inductively Coupled Plasma Mass Spectrometry (ICP-MS) with corresponding instruments of ICP-AES 5300 DV and ICP-MS NexION300D, respectively with an analytical accuracy of ±0.5% and detection limit of 2 ηg/L. The ions (anions and cations) were tested by the Water Isotope and Water-Rock Interaction Laboratory of the Institute of Geology and Geophysics, Chinese Academy of Sciences (IGGCAS-WRIL). The anions (including F^-, Cl^-, NO_3^-, SO_4^{2-}) were analyzed by IC (ISC 1100, ThermoFisherScientific, detection limit: 0.05 mg/L). The main cations (K^+, Na^+, Ca^{2+} and Mg^{2+}) were analyzed by ICP-AES (ICAP6000, ThermoFisherScientific, detection limit: 0.01 mg/L). The calculated ionic charge balance was less than ±5% for most samples and some were within ±10%. In addition, the $\delta^{18}O$ and δ_D were analyzed by the water isotope analyzer Picarro L2101-i in IGGCAS-WRIL, and the precisions of the $\delta^{18}O$ and δ_D values were ±0.03% and ±0.5%, respectively. Details of the analysis of both can be found in Luo et al. (2022) and Tian et al. (2021). Data on hydrochemistry result and REEs result can be found in Table 1 and Table 2, and the $\delta^{18}O_{H2O}$ and $\delta^{2}H_{H2O}$ results are listed in Table 3.

4. Results

4.1. Hydrogeochemistry

The geochemical analysis results for the collected samples are listed in Table 1. The pH of all thermal water and cold water (including river

Table 1
The geochemical analysis results in the study area.

Sample ID	Sample type	T (°C)	pH	F^- mg/L	Cl^-	NO_3^-	SO_4^{2-}	Na^+	K^+	Mg^{2+}	Ca^{2+}	CO_3^{2-}	HCO_3^-	SiO_2	Al μg/L	TDS mg/L	water type	ICB (%)
XZ01	spring	88.9	7.22	4.6	1473.9	0.0	96.0	861.8	47.1	0.5	152.8	0.0	68.8	101.4	6.9	2772.4	Cl-Na	−1.22
XZ02	thermal well	98	7.57	4.1	1544.2	0.0	108.7	870.1	51.7	0.5	166.2	0.0	72.5	113.6	15.6	2781.8	Cl-Na	0.07
XZ03	thermal well	90	7.72	4.0	1640.5	0.0	104.9	917.4	52.6	0.5	172.8	0.0	76.3	118.8	16.5	2930.9	Cl-Na	0.39
XZ04	thermal well	99.4	7.58	4.2	1619.7	0.0	106.1	889.9	52.7	0.5	173.8	0.0	67.5	119.5	28.7	2880.8	Cl-Na	0.83
XZ05	thermal well	90	7.47	4.1	1592.2	0.0	104.8	896.3	52.8	0.5	173.8	0.0	75.1	135.6	24.9	2862.1	Cl-Na	−0.16
XZ07	thermal well	85.6	7.89	4.7	1306.5	0.0	92.0	741.8	45.3	0.5	122.5	0.0	82.6	118.8	32.3	2354.7	Cl-Na	1.27
SZ08	thermal well	80	7	4.8	5101.5	0.0	211.5	2433.9	124.7	9.8	852.4	0.0	0.0	71.3	42.2	8809.8	Cl-Na-Ca	−0.76
SZ09	thermal well	61	7.33	5.1	5297.3	0.0	206.9	2585.6	133.9	10.5	922.2	0.0	0.0	63.8	31.6	9225.3	Cl-Na-Ca	−2.25
SZ10	thermal well	75	7.34	4.9	4691.1	0.0	202.3	2386.7	123.9	9.2	808.9	0.0	0.0	63.8	25.1	8290.9	Cl-Na-Ca	−3.46
SZ11	spring	71	7.24	5.6	4867.3	0.0	207.9	2520.4	121.3	8.9	790.0	0.0	0.0	63.8	20.2	8585.1	Cl-Na-Ca	−3.22
MM13	thermal well	76.4	7.68	7.8	728.4	0.0	73.5	420.0	18.9	0.3	79.9	0.0	72.5	78.7	24.8	1443.7	Cl-Na	1.66
MM14	thermal well	81	7.78	7.3	708.0	0.0	70.7	399.0	18.1	0.3	76.9	0.0	80.1	79.7	17.9	1399.9	Cl-Na	2.99
MM17	thermal well	77	6.77	4.5	5618.2	0.0	213.3	2592.1	103.7	14.1	1164.0	0.0	93.8	104.1	15.9	9861.0	Cl-Na-Ca	−2.41
MM18	thermal well	80	7.27	4.7	5460.9	0.0	205.0	2469.7	101.4	13.9	1139.3	0.0	85.1	100.7	24.3	9538.1	Cl-Na-Ca	−1.94
MM20	thermal well	62	8.37	11.8	142.8	0.0	40.0	173.0	6.3	0.1	6.8	12.0	146.3	104.5	19.2	564.4	Cl-HCO_3-Na	−2.01
HZ22	thermal well	54.7	7.49	8.7	51.2	0.0	88.3	203.0	16.2	1.8	41.6	0.0	544.1	119.1	11.4	801.9	HCO_3-Na	3.17
HZ23	thermal well	99	7.88	14.3	58.5	0.0	111.7	240.0	18.3	0.4	12.7	0.0	594.2	186.9	29.7	940.0	HCO_3-Na	8.55
HZ24	thermal well	48	7.82	6.7	21.2	0.0	41.4	176.8	7.0	1.4	19.1	0.0	449.1	77.9	20.8	576.1	HCO_3-Na	−0.65
HZ26	thermal well	52	7.66	11.3	29.2	0.0	55.8	194.2	12.0	1.1	22.4	0.0	457.8	121.7	31.5	676.7	HCO_3-Na	−2.37
HZ27	thermal well	49	8.32	10.6	31.5	0.0	61.9	202.0	12.7	1.2	24.4	0.0	452.8	148.3	20.5	718.9	HCO_3-Na	−4.06
HZ28	thermal well	50	7.13	6.6	5.9	0.0	13.0	47.8	4.3	2.6	24.6	0.0	178.9	91.7	11.0	286.0	HCO_3-Na-Ca	−3.72
HZ29	thermal well	51.8	8.15	8.7	30.1	0.0	61.5	228.1	13.3	2.2	40.6	0.0	545.4	77.9	31.4	735.1	HCO_3-Na	−5.90
HZ30	thermal well	50	7.49	9.3	25.4	0.0	54.6	203.0	15.2	5.5	23.9	0.0	673.0	33.7	21.4	707.1	HCO_3-Na	8.52
HZ32	thermal well	50	7.12	8.8	32.5	0.0	58.0	180.7	14.3	1.4	34.3	0.0	634.2	60.4	15.1	707.4	HCO_3-Na	11.00
HZ33	thermal well	60	8.61	17.3	10.8	0.0	12.3	83.7	2.4	0.2	3.6	9.0	161.4	77.1	32.9	292.6	HCO_3-Na	−5.25
HZ34	spring	61	8.46	18.5	11.7	0.0	14.9	86.1	2.6	0.4	4.7	9.0	146.3	293.1	19.8	509.7	HCO_3-Na	−9.93
HZ35	thermal well	56	8.1	13.7	13.3	0.0	36.2	129.0	5.1	0.3	11.3	0.0	251.4	105.4	20.7	440.0	HCO_3-Na	−9.24
HZ36	thermal well	48	7.05	4.0	942.6	0.0	102.2	528.7	12.9	1.3	187.9	0.0	102.6	67.2	11.9	1898.2	Cl-Na	−3.28
HZ37	thermal well	41	7.78	0.9	3.4	0.0	90.6	6.0	1.9	5.5	64.1	0.0	121.3	23.8	10.9	256.8	HCO_3-SO_4-Ca	0.05
HZ38	spring	54	7.31	6.9	13.6	0.0	260.2	128.6	7.6	2.5	63.8	0.0	195.1	108.9	15.3	689.6	SO_4-HCO_3-Na-Ca	−0.95
HZ39	thermal well	52	7.51	9.0	8.4	0.0	55.7	61.8	3.9	1.7	35.9	0.0	195.1	80.1	11.1	354.1	HCO_3-SO_4-Na-Ca	−1.35
HZ40	thermal well	54	7.92	3.5	5.4	0.0	532.9	81.0	5.5	4.1	164.4	0.0	90.1	85.7	15.0	927.6	SO_4-Ca-Na	2.02
HZ41	thermal well	66.8	8.24	9.2	11.0	0.0	23.7	117.4	5.0	0.9	26.9	0.0	321.5	93.4	9.4	448.2	HCO_3-Na	−4.49
HZ42	thermal well	54	8.2	11.9	7.4	0.0	18.1	94.8	3.6	0.3	10.6	0.0	228.9	110.6	8.9	371.8	HCO_3-Na	−4.75
HZ43	thermal well	42	7.53	1.8	4.0	2.4	14.2	11.2	1.4	4.5	51.1	0.0	153.8	20.2	7.5	187.6	HCO_3-Na	−8.14
FS01	thermal well	80.1	8.03	12.8	12.2	0.0	7.7	97.7	3.9	0.1	3.9	0.0	240.7	98.1	–	356.8	HCO_3-Na	−1.07
FS02	thermal well	78	8.02	12.3	9.8	0.0	8.2	90.4	3.9	0.1	3.5	0.0	232.0	89.1	–	333.3	HCO_3-Na	0.48
FS03	thermal well	53.6	7.93	5.7	26.4	0.3	15.5	96.3	3.1	0.0	4.2	0.0	227.1	55.5	–	320.5	HCO_3-Na	3.40
FS04	thermal well	63	8.22	9.8	17.1	14.8	9.6	86.6	4.1	0.1	4.1	3.7	206.0	88.7	–	339.8	HCO_3-Na	1.27
FS05	thermal well	72	–	12.2	12.8	0.4	5.9	98.6	4.0	0.1	4.3	0.0	249.4	94.1	–	357.1	HCO_3-Na	−0.39
FS06	thermal well	52	7.46	8.6	156.4	0.0	11.9	221.0	9.5	0.0	13.0	0.0	446.7	111.6	–	755.4	HCO_3-Cl-Na	6.80
FS07	thermal well	65.9	8.36	9.6	167.9	0.6	18.7	152.5	4.8	0.0	4.6	0.0	171.2	85.3	–	529.6	Cl-HCO_3-Na	6.74
FS08	thermal well	60.5	8.03	9.4	166.2	0.0	18.1	152.8	4.5	0.0	4.8	0.0	174.9	82.7	–	526.0	Cl-HCO_3-Na	6.63
FS09	thermal well	67	7.97	9.7	168.6	0.0	18.8	153.8	4.9	0.0	4.9	0.0	178.7	85.9	–	536.0	Cl-HCO_3-Na	7.10
FS10	thermal well	45.6	7.46	6.9	25.4	2.4	21.7	76.4	3.2	0.2	7.3	0.0	196.0	52.9	–	294.4	HCO_3-Na	7.40
FS11	thermal well	61	7.92	8.1	25.5	0.5	19.5	86.0	2.9	0.1	6.2	0.0	201.0	58.1	–	307.4	HCO_3-Na	3.48
FS12	thermal well	49	8.18	10.7	14.5	0.0	9.7	97.1	3.4	0.1	3.8	0.0	228.3	56.8	–	310.3	HCO_3-Na	−1.67
FS13	thermal well	84	8.49	19.4	9.8	0.0	7.9	92.4	3.9	0.0	1.9	7.3	182.4	101.1	–	331.3	HCO_3-Na	−6.79
FS14	thermal well	55.3	8.41	15.4	16.2	0.0	8.3	90.8	4.6	0.1	3.3	0.0	202.2	100.5	–	340.3	HCO_3-Na	−3.52
FS15	spring	60.3	8.46	18.9	20.0	0.3	9.7	112.9	4.5	0.1	1.9	0.0	228.3	75.9	–	358.4	HCO_3-Na	−6.34
FS16	spring	58.3	8.23	22.6	19.6	0.0	15.2	136.6	6.3	0.0	1.0	13.4	249.4	108.4	–	441.1	HCO_3-Na	−6.40
FS17	thermal well	48	8.28	18.4	11.8	0.5	9.4	82.0	4.3	0.0	1.6	4.9	147.6	93.0	–	297.3	HCO_3-Na	−9.36
FS18	thermal well	96	8.59	17.8	11.5	0.5	9.0	79.6	4.2	0.0	1.6	4.9	147.6	90.4	–	290.9	HCO_3-Na	−8.15

(*continued on next page*)

Table 1 (*continued*)

Sample ID	Sample type	T (°C)	pH	F^- mg/L	Cl^-	NO_3^-	SO_4^{2-}	Na^+	K^+	Mg^{2+}	Ca^{2+}	CO_3^{2-}	HCO_3^-	SiO_2	Al μg/L	TDS mg/L	water type	ICB (%)
FS19	spring	82	8.47	16.1	6.6	0.0	5.0	67.7	1.7	0.0	1.2	4.9	122.8	81.9	–	244.1	HCO_3-Na	−10.49
FS20	thermal well	94	8.31	19.2	10.4	0.0	13.6	83.5	2.2	0.0	1.3	7.3	120.4	73.7	–	267.8	HCO_3-Na	−14.60
FS21	thermal well	89	8.39	12.9	7.5	0.3	25.3	80.7	1.8	0.0	1.1	3.7	137.7	61.7	–	262.0	HCO_3-Na	−7.28
FS22	thermal well	47	8.78	15.1	19.7	0.4	17.9	98.0	4.8	0.1	4.1	0.0	213.4	94.7	–	361.5	HCO_3-Na	−1.81
FS23	thermal well	62	8.84	10.2	9.1	0.3	8.8	76.5	3.2	0.1	4.6	0.0	188.6	64.9	–	272.0	HCO_3-Na	−1.55
FS24	thermal well	63	8.84	12.8	18.3	4.3	16.5	87.8	3.8	0.2	4.8	0.0	184.9	73.3	–	314.3	HCO_3-Na	−3.39
FS25	thermal well	55	8.33	16.3	21.6	0.3	12.4	108.8	4.2	0.1	3.0	0.0	239.5	82.5	–	369.0	HCO_3-Na	−1.99
FS26	thermal well	60	8.26	22.1	19.5	0.4	16.2	135.5	6.3	0.0	1.2	8.5	251.9	104.6	–	436.0	HCO_3-Na	−7.09
FS27	cold groundwater well	24	6.25	15.3	16.2	0.0	8.1	91.4	4.6	0.1	3.4	0.0	208.4	101.8	–	345.1	HCO_3-Na	−2.67
FS28	thermal well	35	7.96	19.1	20.1	0.4	10.1	113.9	4.5	0.0	1.8	0.0	229.5	75.4	–	360.1	HCO_3-Na	−6.48
FS29	cold spring	22	7.42	0.2	9.6	11.5	6.4	10.8	7.1	0.7	3.0	0.0	25.5	27.9	–	90.0	HCO_3-Cl-Na	−2.03
FS30	thermal well	49.5	7.98	0.1	1.6	1.8	1.2	4.1	2.1	0.0	0.2	0.0	9.9	20.5	–	36.6	HCO_3-Na	−2.94
FS31	river	–	7.67	0.2	5.8	6.0	15.5	6.9	3.0	0.9	5.5	0.0	15.9	9.8	–	61.6	SO_4-HCO_3-Na-Ca	1.51
FS32	river	–	8.05	0.2	6.3	6.8	15.8	7.0	3.0	0.9	5.8	0.0	13.4	8.4	–	60.9	SO_4-HCO_3-Na-Ca	−1.18
FS33	river	–	7.67	0.2	4.8	6.5	4.1	5.8	3.8	0.5	4.8	0.0	22.4	12.3	–	54.0	HCO_3-Na-Ca	−3.40
FS34	river	–	7.47	0.8	5.9	5.7	15.4	9.9	3.8	0.5	7.0	0.0	27.8	14.0	–	76.9	HCO_3-SO_4-Na-Ca	1.37
FS35	river	–	7.48	0.8	19.8	9.1	17.8	22.0	5.6	0.5	6.4	0.0	36.6	13.8	–	114.1	HCO_3-Cl-Na	2.49

Note: - means below the detection limit or no test; ICB means ions charge balance.

and cold groundwater) samples collected from the five geothermal fields differ slightly, ranging from 6.25 to 8.84 and the water is neutral or weakly alkaline. Temperatures of the thermal water in the XZ geothermal field are all higher than 80 °C, which is the highest compared to other geothermal fields. For the MM and SZ geothermal fields, temperatures of thermal water vary from 60 to 80 °C, while that for HZ and FS fields was 40–100 °C.

A piper diagram Fig. 2 showed that the geothermal water can be divided into Cl–Na type represented by the XZ, SZ, and MM geothermal fields, and HCO_3–Na type water represented by the HZ and FS geothermal fields. For the cold waters, the cations are mainly Na^+, but anions are complicated, among which HCO_3^- constitutes the most critical part and SO_4^{2-} predominates in some samples as well (such as FS31, FS32). For geothermal waters, the main ion components change with the total dissolved solids (TDS). In the coastal XZ, SZ, and MM geothermal fields, water is mainly composed of Na^+ and Cl^- with higher TDS, especially for samples from the SZ and MM fields like MM17, MM18 with extremely high TDS even exceeding 8000 mg/L, which belongs to brine water or salty water. However, as it gradually gets farther from the sea, the component of thermal water in the HZ and FS fields becomes HCO_3^- and Na^+ predominant with lower TDS values, almost less than 1000 mg/L classified as freshwater.

Except for some samples in HZ that are Ca^{2+} dominated, cation compositions of all geothermal waters in the study area are Na^+ dominated, which may be related to the large-scale decarbonation that took place during the natural process of hot water ascending into springs or the anthropogenic extraction of geothermal wells. Besides, the white sinter observed at many sampling sites (i.e., XZ02, XZ04, HZ23) during field sampling also confirmed this speculation. On the other hand, the geothermal anions in XZ, SZ, and MM are dominated by Cl^-, while in the HZ and FS fields they are dominated by HCO_3^-. MM, XZ, and SZ geothermal fields are closer to the sea than the HZ and FS fields as depicted in Fig. 1. It is inferred that the groundwaters of XZ, SZ, and MM may be largely affected by the mixing of seawater, thus forming the major Cl-Na type water with Cl^- as the main anion. From the coast to inland areas such as HZ and FS, geothermal water has gradually changed from the Cl–Na type to the HCO_3/CO_3–Na type.

4.2. REEs

The concentration of REEs dissolved in the water displays a narrow variation ranging from 0.011 to 1.103 μg/L with an average of 0.240 μg/L (Table 2). REEs' differentiation for any researched geothermal field shows that the average concentration of summarized HREEs (ΣHREEs, ΣEr-Lu+*Y*, the 'Σ' signal here represents the total concentration of several elements) ranks first, followed by ΣLREEs (ΣLa-Nd), and that of MREEs (ΣMREEs, ΣSm-Ho) is the minimum. Simultaneously, the ratios of ΣLREEs/ΣHREEs in all collected water samples are between 0.04 and 5.33, with an average value of 0.96. Except for some cold-water samples with larger ΣLREEs/ΣHREEs, the geothermal water almost shows up as ΣLREEs/ΣHREEs<1, thus implying a prevalent enrichment of HREEs relative to LREEs for most of the geothermal water in these typical geothermal fields in Guangdong Province.

The previous studies revealed that the Post Archaean Australian Shale (PAAS) standardized treatment of REEs was commonly used in groundwaters, river waters and seawaters and it can well reflect the characteristics of REEs variation trend of groundwaters (Guo, 2018; Larsen et al., 2021; Yuan et al., 2014). Herein, REEs normalization to PAAS standard (McLennan, 2018) is shown in Fig. 3, and detailed raw data processing of rock samples is listed in Table S1. Certain diversities are existing in REEs' differentiation from different geothermal fields. REEs of water samples in the same geothermal field basically possess the same characteristics of distribution modes (Fig. 3a-e) indicating that similar water-rock interactions are being experienced. All the five thermal fields present a left-leaning type of REEs differentiation mode with more enriched HREEs than LREEs as well as a significant positive

Table 2
The results of REEs in the study area.

Sample ID	Sample type	T (°C)	pH	La μg/L	Ce	Pr	Nd	Sm	Eu	Gd	Tb	Dy	Y	Ho	Er	Tm	Yb	Lu	ΣREE	ΣLREE	ΣHREE	ΣLREE/ΣHREE
XZ01	spring	88.9	7.2	0.017	0.012	<0.002	0.007	0.007	0.005	0.006	<0.002	<0.002	0.077	<0.002	0.003	<0.002	0.016	<0.002	0.15	0.048	0.102	0.471
XZ02	thermal well	98	7.6	0.01	0.011	<0.002	0.016	0.015	0.018	0.012	<0.002	0.017	0.058	<0.002	0.003	<0.002	0.023	<0.002	0.183	0.07	0.113	0.619
XZ03	thermal well	90	7.7	0.005	0.008	0.004	0.008	<0.002	0.006	<0.002	0.004	0.012	0.054	0.002	0.003	<0.002	<0.002	0.002	0.108	0.031	0.077	0.403
XZ04	thermal well	99.4	7.6	0.011	0.018	0.004	0.008	0.007	0.018	0.006	<0.002	0.012	0.052	0.002	0.009	<0.002	0.009	0.002	0.158	0.066	0.092	0.717
XZ05	thermal well	90	7.5	0.014	0.019	<0.002	0.022	<0.002	0.008	0.018	0.002	<0.002	0.055	<0.002	<0.002	<0.002	<0.002	0.003	0.141	0.063	0.078	0.808
XZ06	cold groundwater well	–	7.1	0.016	0.013	0.006	0.029	0.007	0.005	0.005	0.002	0.016	0.022	<0.002	0.003	0.004	<0.002	<0.002	0.128	0.076	0.052	1.462
XZ07	thermal well	85.6	7.9	0.013	0.02	0.006	<0.002	<0.002	0.004	0.012	0.005	0.012	0.051	<0.002	0.003	<0.002	<0.002	0.002	0.128	0.043	0.085	0.506
SZ08	thermal well	80	7	0.028	0.018	0.008	0.035	<0.002	0.046	<0.002	0.002	<0.002	0.162	0.003	0.007	0.003	0.005	<0.002	0.317	0.135	0.182	0.742
SZ09	thermal well	61	7.33	0.007	0.004	0.005	0.009	<0.002	0.031	0.014	<0.002	0.014	0.113	0.003	<0.002	0.004	0.011	0.004	0.219	0.056	0.163	0.344
SZ10	thermal well	75	7.34	0.011	0.021	<0.002	0.038	0.009	0.01	0.015	0.002	0.015	0.168	0.007	0.008	0.003	0.023	0.003	0.333	0.089	0.244	0.365
SZ11	spring	71	7.24	0.014	0.005	0.006	0.027	0.018	0.02	0.02	0.003	0.007	0.158	0.008	0.011	0.002	0.017	0.012	0.328	0.09	0.238	0.378
SZ12	seawater	–	–	0.012	0.008	0.011	0.035	0.009	0.002	0.013	0.004	0.006	0.119	0.023	0.008	<0.002	0.039	0.005	0.294	0.077	0.217	0.355
MM13	thermal well	76.4	7.7	0.007	0.008	<0.002	0.039	<0.002	0.002	0.006	<0.002	<0.002	0.04	0.008	<0.002	<0.002	0.005	<0.002	0.115	0.056	0.059	0.949
MM14	thermal well	81.0	7.8	0.007	0.021	0.007	0.017	<0.002	<0.002	0.006	<0.002	0.013	0.045	0.008	<0.002	0.004	0.004	0.002	0.134	0.052	0.082	0.634
MM15	spring	79.0	8.9	0.005	0.026	0.005	0.008	0.015	0.011	0.016	0.003	0.017	0.014	<0.002	0.003	<0.002	<0.002	<0.002	0.123	0.07	0.053	1.321
MM17	thermal well	77.0	6.8	0.063	0.077	0.013	0.058	0.007	0.049	0.021	0.007	0.062	0.494	0.013	0.018	0.004	0.032	0.003	0.921	0.267	0.654	0.408
MM18	thermal well	80.0	7.3	0.022	0.016	0.007	0.031	0.016	<0.002	<0.002	0.005	0.005	0.15	0.005	0.003	<0.002	0.025	0.009	0.294	0.092	0.202	0.455
MM19	river	25.0	6.6	0.039	0.141	0.007	0.045	0.016	0.011	0.012	0.006	0.012	0.015	0.003	0.006	<0.002	<0.002	<0.002	0.313	0.259	0.054	4.796
MM20	thermal well	62.0	8.4	0.015	0.019	0.004	0.03	0.024	0.009	0.012	0.002	0.024	0.043	0.003	0.01	0.004	0.004	0.002	0.205	0.101	0.104	0.971
YZ21	seawater	27.8	7.9	0.026	<0.002	0.01	<0.002	0.017	0.005	0.024	0.004	0.013	0.072	0.028	0.003	0.005	0.011	0.002	0.22	0.058	0.162	0.358
HZ22	thermal well	54.7	7.49	0.029	0.072	0.004	0.034	<0.002	0.014	0.024	0.003	0.077	0.631	0.012	0.054	0.01	0.043	0.006	1.013	0.153	0.86	0.178
HZ23	thermal well	99	7.88	0.004	0.019	0.007	0.007	0.008	0.006	0.02	0.002	0.019	0.198	0.009	0.02	0.007	0.011	0.006	0.343	0.051	0.292	0.175
HZ24	thermal well	48	7.82	0.003	0.009	0.003	0.014	<0.002	0.006	0.011	<0.002	<0.002	0.059	<0.002	0.007	0.003	0.005	0.003	0.123	0.035	0.088	0.398
HZ25	cold groundwater well	32	6.77	0.006	0.015	<0.002	0.006	0.014	0.019	0.009	<0.002	<0.002	0.011	<0.002	0.004	<0.002	0.006	<0.002	0.09	0.06	0.03	2.000
HZ26	thermal well	52	7.66	0.015	0.035	0.004	0.02	0.029	0.017	0.01	0.006	0.016	0.219	0.012	0.018	0.004	0.034	0.005	0.444	0.12	0.324	0.370
HZ27	thermal well	49	8.32	0.005	0.031	0.01	0.026	0.014	0.006	0.004	0.003	0.004	0.13	0.004	0.003	0.008	<0.002	<0.002	0.248	0.092	0.156	0.590
HZ28	thermal well	50	7.13	0.021	0.027	0.003	0.026	0.007	0.004	0.004	<0.002	<0.002	0.048	<0.002	0.007	<0.002	0.01	0.005	0.162	0.088	0.074	1.189
HZ29	thermal well	51.8	8.15	0.01	0.044	0.002	0.013	0.007	0.016	0.018	0.004	0.016	0.244	0.003	0.011	0.003	0.011	0.003	0.405	0.092	0.313	0.294
HZ30	thermal well	50	7.49	0.005	0.013	<0.002	0.006	<0.002	0.006	<0.002	0.003	0.005	0.073	0.006	0.017	0.003	0.01	<0.002	0.147	0.03	0.117	0.256
HZ31	surface water	–	7.89	0.035	0.217	0.008	0.049	<0.002	<0.002	0.011	<0.002	<0.002	0.03	0.005	0.012	<0.002	<0.002	<0.002	0.367	0.309	0.058	5.328
HZ32	thermal well	50	7.12	0.021	0.033	0.002	0.019	0.007	0.01	0.014	<0.002	0.011	0.249	0.005	0.018	0.004	0.016	<0.002	0.409	0.092	0.317	0.290
HZ33	thermal well	60	8.61	0.003	0.015	0.005	0.013	<0.002	0.005	0.014	<0.002	0.011	0.018	0.002	0.004	<0.002	0.01	<0.002	0.1	0.041	0.059	0.695
HZ34	spring	61	8.46	0.008	0.018	0.004	0.007	0.008	0.004	0.005	0.003	<0.002	0.023	<0.002	0.004	<0.002	0.018	0.002	0.104	0.049	0.055	0.891
HZ35	thermal well	56	8.1	0.003	0.03	0.006	0.019	<0.002	0.007	0.004	0.003	0.043	0.266	0.01	0.011	0.003	0.021	0.005	0.431	0.065	0.366	0.178
HZ36	thermal well	48	7.05	0.026	0.068	0.007	0.026	0.007	0.023	<0.002	0.002	0.011	0.185	0.002	0.01	<0.002	0.021	0.007	0.395	0.157	0.238	0.660
HZ37	thermal well	41	7.78	0.002	0.011	<0.002	0.012	0.007	0.012	<0.002	<0.002	0.014	0.013	<0.002	<0.002	<0.002	<0.002	<0.002	0.071	0.044	0.027	1.630
HZ38	spring	54	7.31	0.014	0.016	<0.002	0.007	0.008	0.004	0.004	0.002	0.011	0.036	<0.002	0.004	<0.002	0.006	<0.002	0.112	0.049	0.063	0.778
HZ39	thermal well	52	7.51	0.013	0.016	0.007	0.012	<0.002	0.01	0.021	<0.002	0.005	0.014	0.002	0.003	<0.002	0.01	<0.002	0.113	0.058	0.055	1.055
HZ40	thermal well	54	7.92	0.024	0.029	0.002	0.014	0.008	0.004	0.005	0.005	<0.002	0.049	<0.002	0.012	0.003	<0.002	0.002	0.157	0.081	0.076	1.066
HZ41	thermal well	66.8	8.24	<0.002	0.011	0.003	<0.002	0.015	0.008	<0.002	<0.002	<0.002	0.013	<0.002	0.004	<0.002	<0.002	<0.002	0.054	0.037	0.017	2.176
HZ42	thermal well	54	8.2	0.005	0.033	0.004	0.014	0.035	0.005	0.013	<0.002	0.005	0.016	<0.002	0.005	<0.002	0.012	0.002	0.149	0.096	0.053	1.811
HZ43	thermal well	42	7.53	0.011	0.028	0.002	0.013	0.014	0.004	0.009	<0.002	<0.002	0.022	0.002	0.003	0.003	0.005	0.003	0.119	0.072	0.047	1.532
FS01	thermal well	80.1	8.03	0.002	0.002	<0.002	<0.002	<0.002	0.026	0.004	<0.002	0.007	0.12	<0.002	0.003	<0.002	0.008	<0.002	0.172	0.03	0.142	0.211
FS02	thermal well	78	8.02	0.005	0.01	<0.002	0.008	<0.002	0.023	0.004	<0.002	0.009	0.093	0.002	0.004	<0.002	0.008	<0.002	0.166	0.046	0.12	0.383
FS03	thermal well	53.6	7.93	0.004	0.009	<0.002	0.008	<0.002	0.025	0.006	0.002	0.021	0.31	0.005	0.018	0.003	0.015	0.003	0.429	0.046	0.383	0.120
FS04	thermal well	63	8.22	0.005	0.004	<0.002	0.004	<0.002	0.024	<0.002	<0.002	<0.002	0.063	<0.002	0.003	<0.002	0.003	<0.002	0.106	0.037	0.069	0.536
FS05	thermal well	72	–	0.002	0.004	<0.002	<0.002	<0.002	0.028	<0.002	<0.002	0.002	0.053	<0.002	0.002	<0.002	0.002	<0.002	0.093	0.034	0.059	0.576
FS06	thermal well	52	7.46	0.006	0.009	<0.002	0.006	0.003	0.048	0.008	0.004	0.049	0.663	0.014	0.061	0.011	0.077	0.011	0.97	0.072	0.898	0.080
FS07	thermal well	65.9	8.36	<0.002	0.002	<0.002	0.004	<0.002	0.014	0.002	<0.002	0.009	0.157	0.004	0.01	<0.002	0.009	<0.002	0.211	0.02	0.191	0.105
FS08	thermal well	60.5	8.03	<0.002	0.002	<0.002	<0.002	<0.002	0.01	0.004	0.002	0.026	0.25	0.007	0.02	0.003	0.018	0.002	0.344	0.012	0.332	0.036
FS09	thermal well	67	7.97	<0.002	<0.002	<0.002	0.003	<0.002	0.008	0.004	<0.002	0.01	0.145	0.002	0.008	<0.002	0.008	<0.002	0.188	0.011	0.177	0.062
FS10	thermal well	45.6	7.46	0.007	0.005	<0.002	0.005	<0.002	0.054	0.004	<0.002	0.02	0.307	0.008	0.046	0.011	0.105	0.024	0.596	0.071	0.525	0.135
FS11	thermal well	61	7.92	0.002	<0.002	<0.002	<0.002	<0.002	0.027	<0.002	<0.002	0.016	0.267	0.006	0.033	0.007	0.08	0.019	0.457	0.029	0.428	0.068

(*continued on next page*)

Table 2 (*continued*)

Sample ID	Sample type	T (°C)	pH	La μg/L	Ce	Pr	Nd	Sm	Eu	Gd	Tb	Dy	Y	Ho	Er	Tm	Yb	Lu	ΣREE	ΣLREE	ΣHREE	ΣLREE/ΣHREE
FS12	thermal well	49	8.18	0.018	0.014	0.004	0.016	0.005	0.065	0.006	<0.002	0.009	0.085	0.002	0.007	<0.002	0.007	0.002	0.24	0.122	0.118	1.034
FS13	thermal well	84	8.49	0.003	0.002	<0.002	<0.002	<0.002	0.031	<0.002	<0.002	<0.002	0.022	<0.002	<0.002	<0.002	<0.002	<0.002	0.058	0.036	0.022	1.636
FS14	thermal well	55.3	8.41	0.005	0.004	<0.002	0.002	<0.002	0.047	0.002	<0.002	0.003	0.028	<0.002	<0.002	<0.002	<0.002	<0.002	0.091	0.058	0.033	1.758
FS15	spring	60.3	8.46	0.003	<0.002	<0.002	<0.002	<0.002	0.042	<0.002	<0.002	<0.002	0.02	<0.002	<0.002	<0.002	<0.002	<0.002	0.065	0.045	0.02	2.250
FS16	spring	58.3	8.23	0.004	0.005	<0.002	0.004	<0.002	0.008	<0.002	<0.002	0.003	0.018	<0.002	<0.002	<0.002	<0.002	<0.002	0.042	0.021	0.021	1.000
FS17	thermal well	48	8.28	0.005	0.007	<0.002	0.002	<0.002	0.011	<0.002	<0.002	<0.002	0.018	<0.002	<0.002	<0.002	<0.002	<0.002	0.043	0.025	0.018	1.389
FS18	thermal well	96	8.59	0.003	0.007	<0.002	0.003	<0.002	0.009	<0.002	<0.002	<0.002	0.024	<0.002	<0.002	<0.002	<0.002	<0.002	0.046	0.022	0.024	0.917
FS19	spring	82	8.47	0.003	0.005	<0.002	0.002	<0.002	0.011	<0.002	<0.002	<0.002	0.023	<0.002	<0.002	<0.002	<0.002	<0.002	0.044	0.021	0.023	0.913
FS20	thermal well	94	8.31	0.005	0.004	<0.002	0.003	<0.002	0.016	<0.002	<0.002	<0.002	0.013	<0.002	<0.002	<0.002	<0.002	<0.002	0.041	0.028	0.013	2.154
FS21	thermal well	89	8.39	<0.002	<0.002	<0.002	<0.002	<0.002	0.013	<0.002	<0.002	<0.002	0.008	<0.002	<0.002	<0.002	<0.002	<0.002	0.021	0.013	0.008	1.625
FS22	thermal well	47	8.78	<0.002	<0.002	<0.002	<0.002	<0.002	0.002	<0.002	<0.002	0.002	0.016	<0.002	<0.002	<0.002	<0.002	<0.002	0.02	0.002	0.018	0.111
FS23	thermal well	62	8.84	<0.002	<0.002	<0.002	<0.002	<0.002	<0.002	<0.002	<0.002	<0.002	0.011	<0.002	<0.002	<0.002	<0.002	<0.002	0.011	–	0.011	–
FS24	thermal well	63	8.84	<0.002	0.004	<0.002	0.005	<0.002	0.004	<0.002	<0.002	<0.002	0.028	<0.002	<0.002	<0.002	<0.002	<0.002	0.041	0.013	0.028	0.464
FS25	thermal well	55	8.33	0.005	0.006	<0.002	0.005	0.003	0.043	0.004	<0.002	0.009	0.086	0.003	0.004	<0.002	0.004	<0.002	0.172	0.062	0.11	0.564
FS26	thermal well	60	8.26	0.008	0.014	0.002	0.007	<0.002	0.053	0.007	0.003	0.031	0.323	0.008	0.028	0.005	0.032	0.005	0.526	0.084	0.442	0.190
FS27	cold groundwater well	24	6.25	0.043	0.045	0.009	0.038	0.011	0.053	0.01	0.003	0.018	0.181	0.005	0.016	0.003	0.017	0.004	0.456	0.199	0.257	0.774
FS28	thermal well	35	7.96	0.002	<0.002	<0.002	0.003	<0.002	0.004	<0.002	<0.002	<0.002	0.034	<0.002	<0.002	<0.002	<0.002	<0.002	0.043	0.009	0.034	0.265
FS29	spring	22	7.42	0.008	0.004	0.003	0.018	0.002	0.009	0.006	<0.002	0.005	0.031	<0.002	0.002	<0.002	0.003	<0.002	0.091	0.044	0.047	0.936
FS30	thermal well	49.5	7.98	0.015	0.028	0.002	0.013	<0.002	0.033	0.004	<0.002	0.005	0.083	<0.002	0.004	<0.002	0.003	<0.002	0.19	0.091	0.099	0.919
FS31	river	–	7.67	0.061	0.034	0.016	0.057	0.013	0.039	0.02	0.004	0.04	0.329	0.011	0.038	0.007	0.03	0.008	0.707	0.22	0.487	0.452
FS32	river	–	8.05	0.032	0.025	0.007	0.031	0.007	0.04	0.009	0.003	0.03	0.299	0.011	0.036	0.006	0.032	0.006	0.574	0.142	0.432	0.329
FS33	river	–	7.67	0.071	0.031	0.014	0.057	0.011	0.041	0.016	0.002	0.008	0.055	<0.002	0.006	<0.002	0.004	<0.002	0.316	0.225	0.091	2.473
FS34	river	–	7.47	0.024	0.018	0.005	0.016	0.002	0.05	0.002	<0.002	0.003	0.025	<0.002	0.003	<0.002	0.004	<0.002	0.152	0.115	0.037	3.108
FS35	river	–	7.48	0.024	0.017	0.005	0.021	0.003	0.043	0.006	<0.002	0.008	0.05	<0.002	0.01	<0.002	0.011	0.003	0.201	0.113	0.088	1.284

Note: - means below the detection limit or no test.

Table 3
The fraction of seawater mixing ratio of different thermal water samples based on δ_D and $\delta^{18}O$.

Sample ID	T °C	Cl^- mg/L	$\delta^{18}O$ ‰	δ_D ‰	*f* (%) Based on δ_D	*f* (%) Based on $\delta^{18}O$
XZ01	88.9	1473.89	−7.05	−43.83	9.79	10.84
XZ02	98	1544.17	−6.84	−42.55	15.50	16.95
XZ03	90	1640.52	−6.49	−41.31	21.08	27.22
XZ04	99.4	1619.7	−6.89	−42.23	16.97	15.50
XZ05	90	1592.22	−6.66	−41.63	19.66	22.39
XZ07	85.6	1306.54	−6.72	−42.09	17.59	20.53
SZ08	80	5101.46	−5.98	−36.88	40.94	42.26
SZ09	61	5297.27	−5.49	−34.88	49.90	56.58
SZ10	75	4691.1	−5.83	−35.79	45.82	46.42
SZ11	71	4867.29	−5.88	−35.70	46.21	45.18
MM13	76.4	728.39	−7.33	−44.85	5.22	2.75
MM14	81	708.02	−6.99	−43.75	10.16	12.72
MM17	77	5618.19	−7.62	−46.21	−0.90	−5.70
MM18	80	5460.87	−6.46	−39.58	28.83	28.15
MM20	62	142.81	−7.33	−43.71	10.32	2.86
HZ22	54.7	51.17	−7.59	−45.50	2.28	−4.92
HZ23	99	58.55	−7.33	−45.05	4.33	2.65
HZ24	48	21.19	−7.57	−46.05	−0.14	−4.31
HZ26	52	29.2	−7.55	−45.05	4.31	−3.83
HZ27	49	31.48	−7.48	−44.87	5.11	−1.68
HZ28	50	5.94	−7.48	−44.93	4.85	−1.63
HZ29	51.8	30.1	−7.39	−44.18	8.21	0.90
HZ30	50	25.43	−7.79	−46.19	−0.79	−10.70
HZ32	50	32.54	−7.37	−44.26	7.86	1.71
HZ33	60	10.77	−8.03	−48.61	−11.63	−17.77
HZ34	61	11.68	−8.13	−49.06	−13.64	−20.70
HZ35	56	13.29	−7.73	−45.88	0.58	−8.99
HZ36	48	942.58	−7.15	−42.75	14.63	7.89
HZ37	41	3.39	−7.26	−44.45	7.00	4.67
HZ38	54	13.63	−7.72	−45.13	3.94	−8.56
HZ39	52	8.38	−7.19	−41.58	19.87	6.98
HZ40	54	5.38	−7.63	−44.19	8.16	−6.13
HZ41	66.8	11.04	−7.67	−45.02	4.46	−7.27
HZ42	54	7.36	−7.54	−43.17	12.76	−3.26
HZ43	42	3.98	−6.52	−37.74	37.07	26.39
FS01	80.1	12.2	−7.53	−48.40	−10.71	−3.15
FS02	78	9.8	−7.32	−47.05	−4.64	3.08
FS03	53.6	26.39	−6.55	−42.08	17.65	25.50
FS04	63	17.1	−7.31	−46.60	−2.65	3.25
FS05	72	12.8	−7.45	−47.96	−8.75	−0.63
FS06	52	156.4	−7.76	−49.65	−16.28	−9.67
FS07	65.9	167.9	−7.37	−46.98	−4.32	1.50
FS08	60.5	166.2	−7.30	−47.54	−6.84	3.56
FS09	67	168.6	−7.39	−47.45	−6.42	1.13
FS10	45.6	25.4	−6.24	−42.25	16.85	34.49
FS11	61	25.5	−7.12	−45.16	3.83	8.86
FS12	49	14.5	−6.76	−43.27	12.29	19.27
FS13	84	9.8	−7.37	−47.52	−6.74	1.60
FS14	55.3	16.2	−7.66	−48.38	−10.60	−6.87
FS15	60.3	20.0	−7.69	−49.19	−14.22	−7.76
FS16	58.3	19.6	−7.63	−47.83	−8.15	−5.96
FS17	48	11.8	−7.65	−47.92	−8.53	−6.52
FS18	96	11.5	−7.46	−47.58	−7.00	−1.10
FS19	82	6.6	−7.38	−47.39	−6.17	1.36
FS20	94	10.4	−7.58	−48.04	−9.07	−4.49
FS21	89	7.5	−7.33	−47.43	−6.35	2.73
FS22	47	19.7	−7.69	−48.49	−11.08	−7.83
FS23	62	9.1	−7.83	−48.70	−12.03	−11.86
FS24	63	18.3	−8.06	−51.21	−23.30	−18.45
FS25	55	21.6	−7.42	−47.21	−5.38	0.23
FS26	60	19.5	−7.27	−45.77	1.11	4.46
FS28	35	20.1	−7.38	−46.24	−1.03	1.27
FS30	49.5	1.6	−7.72	−48.02	−8.98	−8.67

Eu anomaly and a negative Ce anomaly. Contrary to the REEs speciation pattern of water, that of host rocks is pretty complex (Fig. 3f). For samples R4, R5, and R6, HREEs are more enriched compared to LREEs, while samples R1, and R3 are LREEs-enriched and pertain to an obvious right-leaning type of distribution pattern. The other four samples R2, R7, R8, and R9 but present a relatively flat REE-distribution pattern. This

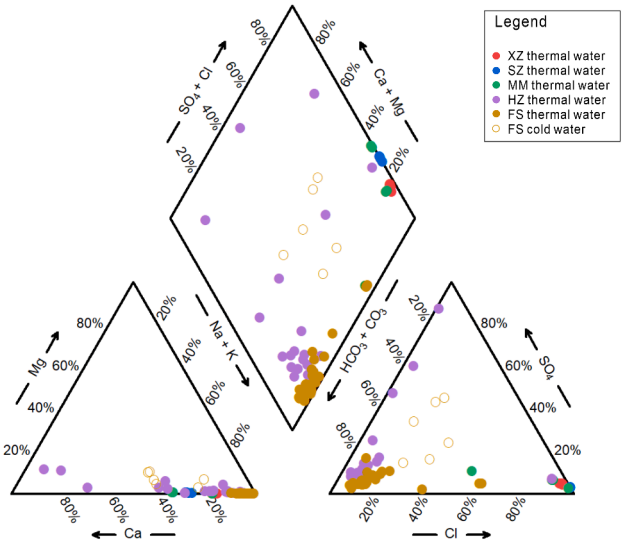

Fig. 2. Piper triangular diagram of major ions dissolved in waters in study area.

great variability indicates a striking contrast manifestation between REEs differentiation modes of waters and that of rocks meaning that the contents and distribution properties of REEs in the water here are not just parent rock dependent. Hence, additional factors controlling REEs will be further discussed in what follows.

5. Discussion

5.1. Controls on REE concentrations

5.1.1. pH

Recent studies note that REEs are sensitive to changes in physicochemical properties in waters (Han et al., 2021), which is mainly reflected in the fact that the contents and distribution modes of REEs may vary quite heterogeneously with spacetime (Zhu, 2017). Existing evidence suggested that pH was among the most important factors fluctuating the REEs in groundwaters. A consensus that the lower pH value tends to correspond to the higher REE concentrations is gradually recognized (Elderfield et al., 1990; Guo et al., 2010; Keasler and Loveland, 1982; Li et al., 2022a; Noack et al., 2014; Wang et al., 2020).

The relationship between REEs and the pH of waters in the five geothermal fields seems to be less pronounced despite the integrally depressed trends for ΣREEs, ΣLREEs, and ΣHREEs (the total concentration of REEs, LREEs, and HREEs, respectively for each sample) along with increasing pH values (Fig. 4a). Now that the pH values of groundwaters vary slightly between 6.25 and 8.84 as mentioned in part 4.1, presumably this narrow range might prevent the pH condition from entirely performing its role in altering the content and fractionation of REEs. Therefore, unlike previous studies characterized by a remarkable contrast for REEs in a widely pH-variable range from the acid to alkaline water (Yuan et al., 2014; Li et al., 2022a), pH does have an effect but not appreciable on REEs in the study area.

The research by Dupré et al. (1996) provided meaningful references for interpreting REEs' dependence on pH and held that the adsorption/desorption process of REEs on the surface of minerals or suspended particles was quite dependent on the pH values, thereby affecting REE concentrations in geothermal waters. Concretely, the lower pH environment was of assistance to the entry of REEs in sediments/rocks into liquids through chemical weathering, thus provoking the accumulation of REEs in groundwaters (Gosselin et al., 1992; Miekeley et al., 1992). On the contrary, the adsorption by the principal carriers of trace elements of metal oxides (such as iron, manganese oxides (Fe/Mn oxides)) or co-precipitation with carbonates (calcites) for dissolved REEs can be triggered accompanied by the gradual neutralization or alkalization of water, thus resulting in the reduction of REEs in groundwaters. On the other hand, this effect under pH influence also counts a great deal in explaining the REEs' fractionation. The always prior sequence for LREEs relative to MREEs and HREEs in the process of adsorption (desorption) with a high (low) level of pH determines the mutually competing enrichment between LREEs and HREEs (Zhu et al., 2005; Liu et al., 2017). In the study area, the neutral or weakly alkaline pH conditions were in favor of the REEs adsorption onto sedimentary surfaces and could cause a decline in REE in groundwater, especially for LREEs. Consistent with this statement, Fig. 3 showed the expected result of HREEs relatively enrichment to LREEs concentrations in waters. Overall, the regulation of pH on the level and differentiation of REEs in groundwater is principally realized through the influence on the

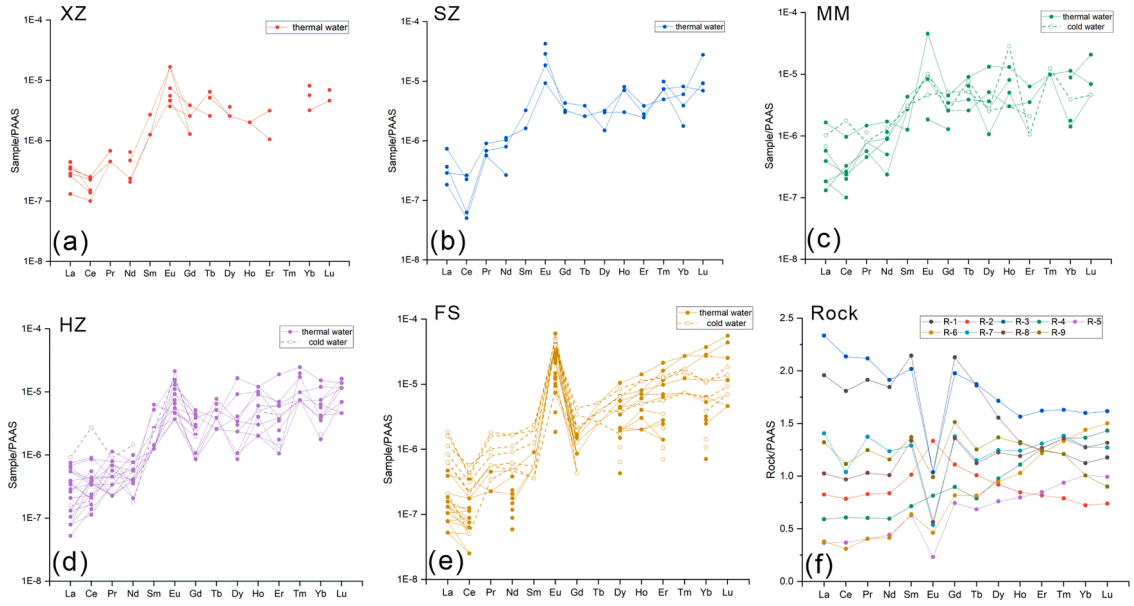

Fig. 3. REEs distribution patterns of water samples (a-e) and host rocks (f) in the study area. The REEs' contents were referenced by Yuan et al. (2014) and Ling et al. (2006).

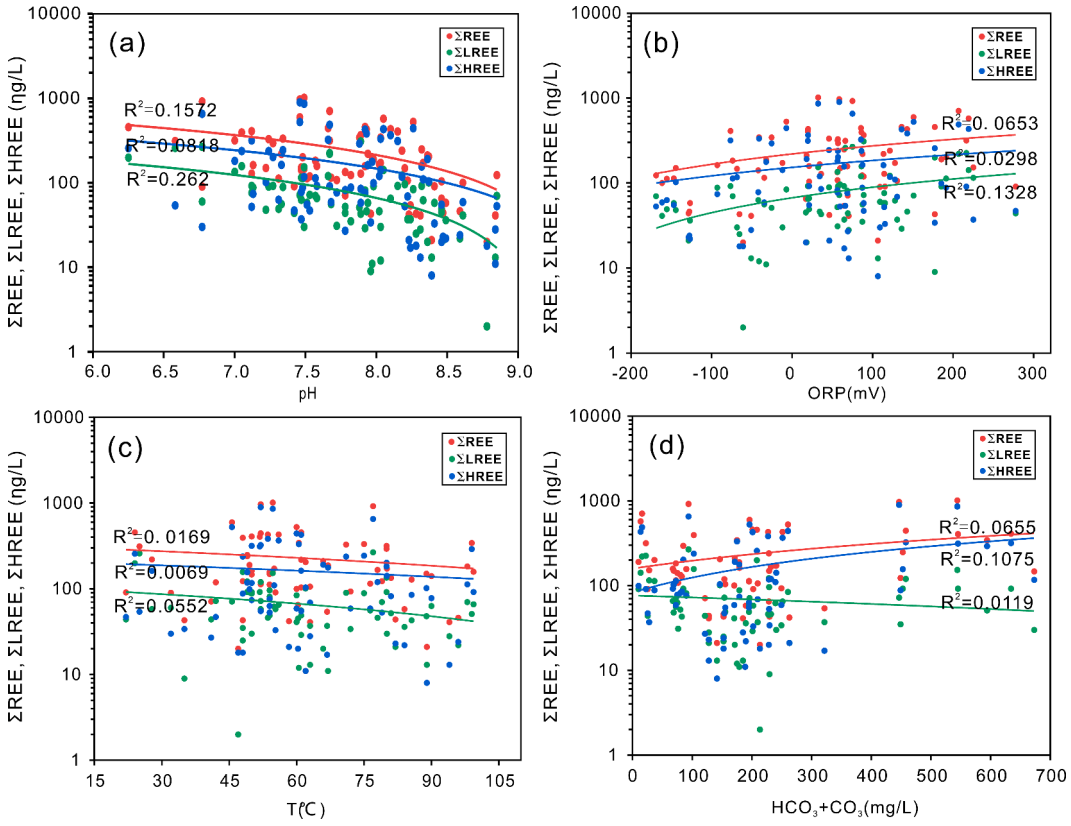

Fig. 4. Relationships between ΣREEs, ΣLREEs, as well as ΣHREEs and different physicochemical parameters ((a) pH, (b) ORP, (c) temperature, and (d) concentrations of HCO_3^- and CO_3^{2-}) in waters in the study area.

adsorption/ desorption of REEs by sediments/ rocks around the water.

5.1.2. Redox conditions

The redox conditions have been proposed to be another significant factor confining the composition and distribution modes of REEs. As an important index parameter of redox conditions, the oxidation–reduction potential (ORP) can represent the oxidation degree of the water body. Generally, the higher the ORP values, the more inclined the water is to oxidative states. From the relationship between ORP values and REEs concentrations (Fig. 4b), it can be found that the ΣREEs, ΣLREEs, and ΣHREEs of groundwaters in the studied geothermal fields relate negatively with the ORP values in spite of a minor relevance indicating a potentially moderate control of ORP on local REEs.

Redox conditions affecting REEs in waters are primarily by way of the modulation of Ce and Eu anomalies due to their attributes as variable valence elements (Dia et al., 2000; Liu et al., 2016). Atypical with the rest of REEs strictly expressed as trivalent in the lanthanide elements group, these two elements can appear in additional valence states (Ce (IV) and Eu(II)), which allows them to be used as available proxies for redox reactions (de Baar et al., 1988; Ma et al., 2019). For example, the Ce negative anomaly in groundwater presumably indicates the oxidation conversion of trivalent Ce(III) to the less soluble tetravalent Ce(IV) preferentially adsorbed to Fe/Mn oxides/oxyhydroxides compared to REE^{3+} (Elderfield and Greaves, 1982; Göb et al., 2013). Thus, in general oxidative waters, Ce often presents a negative anomaly. Conversely, an Eu anomaly was found to occur only in the extremely reducing environment (ORP value < -500 mV, Laveuf and Cornu, 2009) along with the transformation from Eu(III) to Eu (II). Eu (II) has priority to move first over trivalent state REEs, therefore causing strongly positive Eu anomaly in groundwater (Lee et al., 2003; Liu et al., 2016). The detailed discussions on this issue are further involved in the following part 5.2.

Additionally, several studies also held that oscillations of REEs in waters under redox variance may result from the control of adsorption/ desorption of REEs by sediments especially for Fe/ Mn oxyhydroxides (Guo et al., 2010; Verplanck et al., 2004; Ohta and Kawabe, 2001). In a relatively reductive environment, Fe/Mn oxyhydroxides are readily reduced and dissolved into groundwaters. Likewise, REEs attached to the surface of such sediments will also be released and thus increasing their concentrations in waters. To this end, a scatter diagram on the correlation between concentrtions of dissolved Fe+ Mn and ΣREEs for all water samples in the study area was plotted. Fig. 5 showed that REEs increased in phase with the rise of the dissolved Fe+ Mn concentrations showing that the adsorption/desorption of Fe/ Mn oxyhydroxides

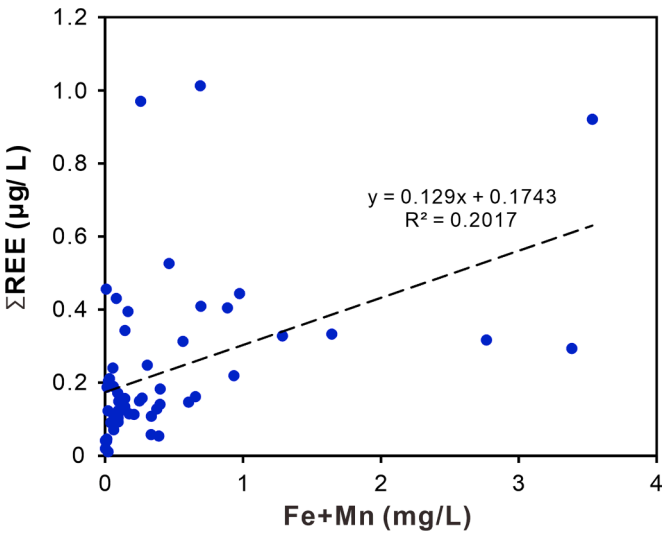

Fig. 5. Plots of ΣREEs and Fe+ Mn contents of waters in the study area.

activated by redox processes did react more or less on the change of REEs in the study area.

5.1.3. Temperature

Previous research has shown that the REEs could have affinities with the temperature of waters and the concentration and distribution pattern of REEs may be discriminated by the variable temperatures in the aqueous environment (Hatipoğlu Temizel et al., 2020; Bulia and Enzweiler, 2018; Bragin et al., 2018; Shakeri et al., 2015). As illustrated in Fig. 3, the distribution pattern of REEs in cold waters was flatter than that in thermal waters. Meanwhile, LREEs concentrations in cold waters seemed to be higher than that in thermal waters, but there was no obvious difference in HREEs concentrations between temperature-disparity waters, which indicated that the near-surface and low-temperature conditions were possibly more conducive to the stable existence of LREEs in groundwaters. And this also illustrated the potentially temperature-interfering role in the REEs' differentiation even though an ambiguous association. As shown in Fig. 4c, the ΣREEs, ΣLREEs and ΣHREEs concentrations in the study area were inconspicuously negatively correlated with the temperature of local groundwaters. Additionally, LREEs concentrations appeared to fluctuate a little more than HREEs concentrations as the temperature changed, which was in line with the results reflected in Fig. 3. Coupling the given information from Fig. 4c and Fig. 3, it is reasonable to infer that the temperature of an aqueous environment is of certain implications to the migration and transformation of REEs and the low temperatures may be partly in operation for the accumulation of REEs, particularly LREEs in fluids.

5.1.4. Complexation reactions

The past decades have seen a considerable effect of the complexation reactions performed in determining the REE concentrations and distribution modes in groundwaters (Ingri et al., 2000; Pourret et al., 2007, 2010; Stern et al., 2007; Wood, 1990). After summarizing pieces of literature (listed below in Figure S2) and a group of reviewed data on the stability constants (LogK) of REEs complexation reactions with different inorganic complexes, it can be intuitively found that compared with inorganic ions such as HCO_3^-/CO_3^{2-}, SO_4^{2-} and F^-, reactions between Cl^-, NO_3^- and REEs in fluids are weaker enough.

The results of some studies suggested that LREEs usually had a higher affinity for suspended particles than HREEs that were complexed more easily by dissolved ligands (Censi et al., 2004; Deng et al., 2017; Sholkovitz, 1992), which can cause a remarkable heterogeneity in the sequence of adsorption and desorption for different REEs and explained well the REEs' differentiation of the enrichment of HREEs relative to LREEs in fluids. Thus, the complexation reactions can determine the REEs' fractionation to a certain extent. Moreover, MREEs or HREEs with smaller atomic radii are accessible to be complexed with enough carbonates in alkaline waters, especially for dicarbonate-bearing species ($Ln(CO_3)_2^-$) (Larsen et al., 2021; Millero, 1992; Nelson et al., 2003). The negatively charged state of this specie makes it difficult to be adsorbed onto the surface of sediments with a negative charge alike. For this reason, MREEs or HREEs mobilize preferentially within fluids relative to LREEs in aqueous systems.

For local geothermal water dominated by HCO_3^-/CO_3^{2-} or Cl^- anions, inorganic complexation reactions between HCO_3^-/CO_3^{2-} and REEs should play an important role in regulating REEs' concentrations and differentiation modes, but the Ln-chloride ligands complexes can be ignored due to their extremely low stability constants (Figure S2). The result in Fig. 4d shows that the concentrations of HCO_3+CO_3 had a minor positive correlation with that of the ΣREEs in local groundwaters. More interestingly, ΣHREEs concentrations increased with the promotion of HCO_3+CO_3 as well, whereas ΣLREEs behaved oppositely. In accordance with the above discussions, we affirmed that the concentrations of free bicarbonates/carbonates (HCO_3^-/CO_3^{2-}) facilitated the rise of REEs/HREEs' concentration and diversifying REEs in local thermal waters, which was possibly due to the widely occurring complexations between HREEs and bicarbonates/carbonates.

5.2. Eu, and Ce anomalies

5.2.1. Origin of Eu anomaly in thermal water

In this study, all the groundwater samples including thermal water from five geothermal fields present a consistent positive Eu anomaly (Table S2). A fair range in Eu anomaly values (Eu/Eu*: 1.10 to 58.45, 12.03 on average) was observed in thermal waters, whereas there was a drastic fluctuation in Eu/Eu* values varying from 3.74 to 117.72 with an average of 29.21 in cold waters. Simultaneously, the Eu enrichment of thermal water in the FS geothermal field was the most prominent than in other thermal fields.

Several generally accepted explanations for the positive Eu anomaly have been given in previous studies mainly including: (1) inheriting the characteristics of Eu anomaly in host rocks (Göb et al., 2013); (2) reduction of Eu^{3+} to Eu^{2+} capable of better migrating within groundwater (Bau, 1991; Lee et al., 2003; Guo et al., 2010); and (3) preferential weathering and dissolution of Eu-rich minerals like feldspars in host rocks (Li et al., 2022b; Hatipoğlu Temizel et al., 2020; Shakeri et al., 2015; McLennan, 2018). Certain chemical characteristics of rocks or sediments in aquifers tend to be inherited by flowing water along with a certain degree of water-rock interaction. However, unlike the intensely negative Eu anomaly presented in the host rocks in the study area (Fig. 3), the water behaved conversely with a positive Eu anomaly. Thus, the REEs behavior here seemed not to be the inheritance of an Eu anomaly from parent rocks. Then, for the purpose of verifying what the influence of redox conditions on the Eu anomaly of waters is, a diagram of the relationship between Eu/Eu* and ORP shows in Fig. 6a. Present studies show that only under strong reducing conditions at temperature >250 °C (Sverjensky, 1984; Hatipoğlu Temizel et al., 2020), ORP value < −500 mV, and pH value of 7 (Laveuf and Cornu, 2009; Liu et al., 2016), Eu^{3+} might be transformed into Eu^{2+} that preferentially migrated within fluids resulting in the positive Eu anomaly in groundwaters. That is to say, the occurrence of Eu reduction generally requires extremely severe environmental conditions, particularly in deep-seated high-temperature reservoirs. However, as shown in Fig. 6a, the more negative the ORP, the closer Eu/Eu* to 1 signifying the weaker positive Eu anomaly in the studied geothermal fields remarkably refuted the contribution of redox conditions to the Eu anomaly here. Excluding the former two assumptions, whether the hypothesis of preferential weathering and dissolution of Eu-rich minerals in host rocks could account for this phenomenon needs to be further explored.

Alkali elements like Li, Rb, and Cs in aqueous solutions are generally stable with only one valence state and without any complexation, assisting in tracking the evolution of hydrothermal systems (Berger et al., 1988). The similar chemical properties of alkali elements make the elemental substitution among them common. For example, Rb and Cs can facilely replace K in K-containing minerals like feldspars or micas. In particular, when these minerals undergo alteration in high-temperature environments, during which Rb and Cs are both likely to be released or incorporated into alteration minerals like clays. Accompanied by the formation of clays, it is widely accepted that Cs will be preferentially adsorbed to its surface compared to Rb (Brouwer et al., 1983; Hart, 1969; Wampler et al., 2012), whereas given the smaller ion radius of Rb relative to Cs, Rb gets priority to access to be incorporated into clays as substitutes for K. These two competing processes together cause the differentiation of Rb/Cs between the minerals retained in place and the altered fluids leached away. A preliminary conclusion was reached by Kizler (2011) that if there were alteration minerals generated from host rocks, both the Rb/Cs ratios of rocks and thermal fluids would decrease. Göb et al. (2013) also found that the strongly altered rocks rich in clay minerals like illite, kaolinite, and chlorite had Rb/Cs ratios ranging from 0.65 to 16.3, with a median value of 3.1, while Rb/Cs ratios of rocks lacking these minerals but containing more intact plagioclases and

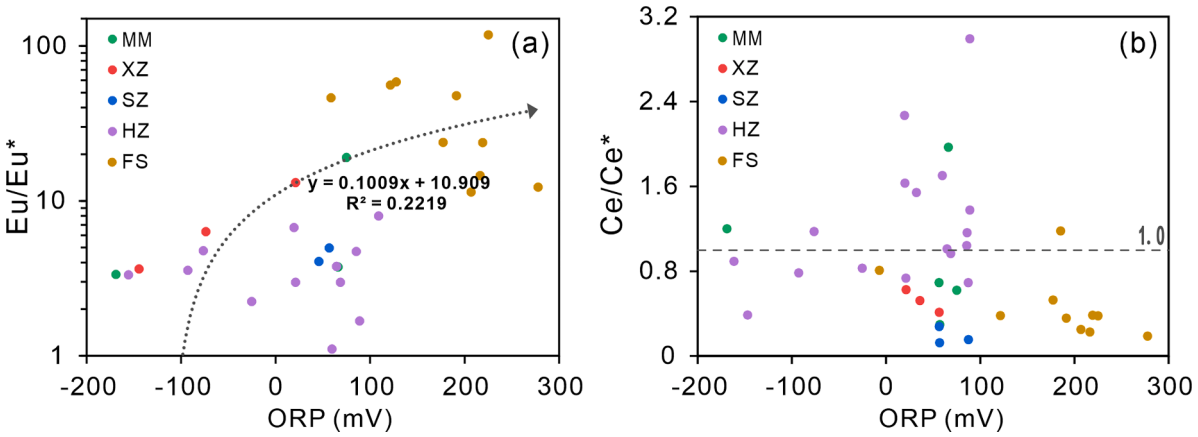

Fig. 6. Relationships between Eu, Ce anomalies and ORP values of waters in the five geothermal fields.

biotites were higher varying between 4.8 and 17.5 with a median value of 7.9. Taking note of the disparate Rb/Cs ratios in separate rocks and the lower Rb/Cs ratio even below 2 in the thermal water, Hatipoğlu Temizel et al. (2020) ascribed this phenomenon to more Rb entering into the newly formed clay minerals after granites had been alternated and sequentially caused the decline of Rb concentration in waters. Thus, the Rb/Cs ratio can also be recognized as a favorable indicator of water-rock interactions.

The concentrations of Rb and Cs in all water samples of the study area were in the range of 0.83–1269 μg/L and 0.038–626 μg/L, respectively (Table S3). Interestingly, Rb/Cs ratios of almost all geothermal water in five geothermal fields were basically below 2 (Fig. 7), presenting less volatility with an average value of 1.6, which seemed to provide a convincing proof for the prevalent occurrence of thermal alteration in local host rocks. Because granites, as the most widely distributed host rocks in the study area, were visible negative Eu anomalies (Fig. 3), it was reasonable to infer that in the process of water-rock interaction, the preferential chemical weathering and dissolution of rocks, alternatively, the argillization/ alteration process of K-rich or Eu-rich minerals like alkaline feldspars (see Eq. (1), K contained in feldspars tended to be isomorphically replaced by Eu, causing the release of K or Eu bearing minerals easily soluble in water altogether with this reaction) to make a large amount of Eu entering into the groundwaters which resulted in the positive Eu anomalies exhibited in the waters but negative Eu anomalies in the host granites (Fig. 3). On the contrary, the cold waters behaved distinctly from the thermal waters in the possession of higher Rb/Cs ratios and a wider variable interval with a maximum value of 177.7. This may be attributable to fewer clays formed in parent rocks, or partially formed clays already reacting with surrounding groundwaters.

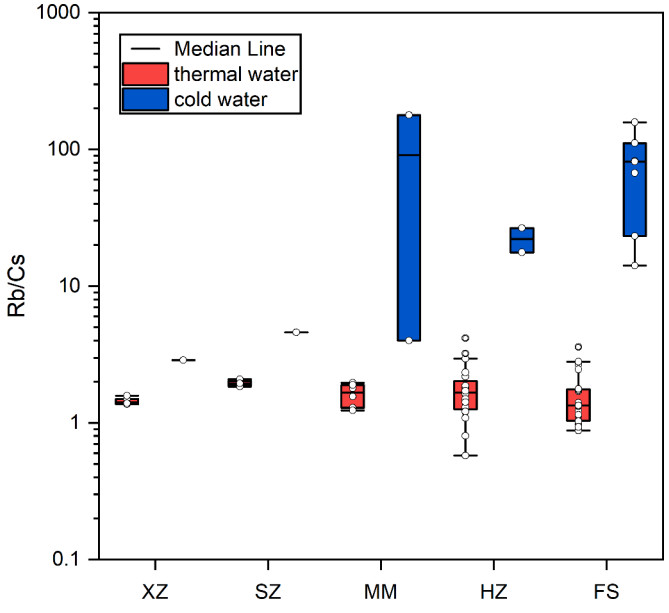

Fig. 7. The Rb/ Cs ratios of waters in the five geothermal fields.

To summarize, it is credible that the thermal waters in the studied geothermal fields presented the positive Eu anomaly primarily originating from the preferential dissolution of Eu-rich minerals, especially feldspars constituted most in granites as the major rock type of local thermal reservoir.

$$2KAlSi_3O_8 + CO_2 + 2H_2O \rightarrow Al_2Si_2O_5(OH)_4 + 2K^+ + CO_3^{2-} + 4SiO_2 \quad (1)$$

5.2.2. Origin of Ce anomaly in thermal water

With a few exceptions in the HZ geothermal field, almost all the thermal waters were characterized by negative Ce anomalies or inconspicuous abnormalities with the value of Ce/Ce* closer to 1. The thermal waters showed similar Ce anomalies as the cold waters, and the Ce/Ce* values were respectively ranging from 0.13 to 2.27 with an average of 0.89 for thermal waters and from 0.19 to 2.99 with an average of 0.81 for cold waters.

Existing research has recognized that the existence of Ce anomaly strongly relies on the redox conditions (Gruau et al., 2004; Miekeley et al., 1992; Deluca et al., 2020). Under environments of low-temperature and oxygen-rich conditions especially in shallow groundwaters, Ce^{3+} is readily oxidized to Ce^{4+} previously adsorbed or complexed on oxides/oxyhydroxides of iron and manganese and thus directly generates the depletion of Ce in fluids (De Carlo et al., 1998; Göb et al., 2013; Guo et al., 2010). Followed by the processes of the oxidative adsorption of iron and manganese (reduction and dissolution of Fe/ Mn oxides/oxyhydroxides), Ce concentrations in waters synchronously decrease (increase), and this implies that the Ce concentrations should be positively correlated with the iron and manganese concentrations.

To examine the causes of Ce anomalies, a cross plot of the ORP and Ce/Ce* values of water was diagrammed (Fig. 6b). It can be seen that the Ce anomalies in the waters had no evident relevance to the ORP values. Moreover, the unexpected negative correlation though slight between concentrations of Ce and iron/manganese illustrated in Fig. 8 still further confirmed that the redox conditions in the local groundwaters did not exert a substantial influence on Ce anomalies.

With the exception of redox conditions, the inheritance of host rocks has also been regarded as one of the causes of Ce anomalies in groundwaters (Smedley, 1991; Johannesson et al., 1999). However, as discussed in the previous part 3.2, the Ce anomalies of granites as the most distributed host rocks were not consistent. R1, R3, and R7

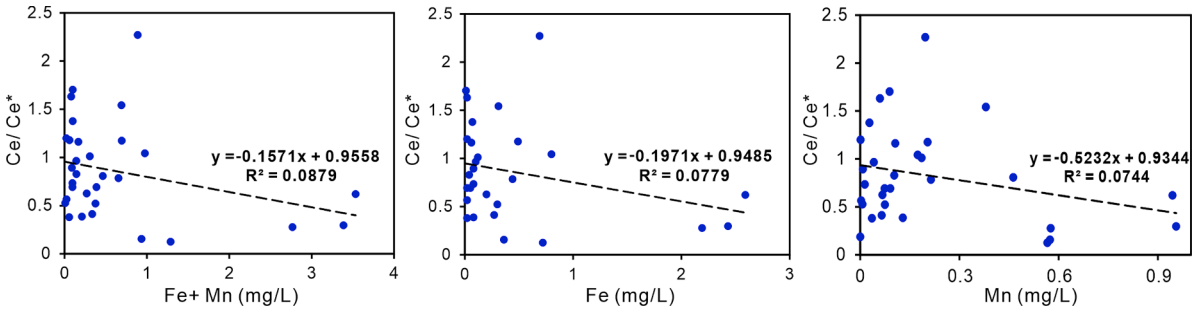

Fig. 8. Relationships between Ce anomalies and contents of Fe+ Mn, Fe, and Mn in waters of the study area.

exhibited obviously negative Ce anomalies, whereas others had no Ce anomalies or a slightly negative Ce anomaly (Fig. 3f). This discordance in behaviors of Ce anomalies between thermal waters and host rocks revealed that the hypothesis of inheritance of host rocks was not convincing enough.

Considering the uniquely coastal geographical location of the geothermal fields in the study area, we suspect that the negative Ce anomalies of geothermal waters can be affected by the mixing of seawater with striking Ce deficits. According to the triangular Na-K-$Mg^{1/2}$ diagram (Figure S1), the thermal waters all lay in a non-equilibrium state indicating insufficient water-rock interactions, which may be possibly due to the occurrence of mixing during the upwelling of thermal water, that is there was possibly an addition of cold water like the local seawater and groundwaters. Fig. 6b shows that the Ce anomalies were obvious in the XZ and SZ geothermal fields as typical coastal regions inferring that thermal waters from these two places may be largely subjected to this effect. The Ce/Ce* values in MM geothermal field behaved as a random distribution. Nevertheless, the sporadic sample collection shows that there is no way to rule out the randomness of such a result. For the HZ and FS geothermal fields, they are relatively farther from the sea and the waters should be less mixed with seawater, and accordingly behave as with slightly more negative Ce anomalies than the other three fields. As expected, the loss of Ce in the HZ geothermal field was not significant, and even some water samples showed positive anomalies, while in the FS field, it showed a noticeably negative Ce anomaly. As stated above, the water near the ground surface with low temperature and rich dissolved oxygen usually presented a characteristic of a negative Ce anomaly resulting from the enhanced oxidative scavenging of Ce from REE^{3+}. Specifically, the oxidized Ce^{4+} readily formed oxyhydroxides of colloidal cerium, and then precipitated and retained in place especially when in neutral or alkaline waters (Loges et al., 2012; Nelson et al., 2003). Consequently, it was speculated that the striking negative Ce anomalies of the thermal water in the HZ geothermal field can be construed by shallow groundwater mixing in the process of thermal water surging towards the surface.

5.3. Seawater mixing and its potential influence on REEs

5.3.1. Evidence of seawater mixing

In light of the previous analyses, it was believed that the seawater intrusion certainly yielded a significant effect on the local geothermal waters. Herein, more persuasive evidence from both qualitative and quantitative views was complemented to affirm the occurrence of mixing processes between the seawater and local fresh groundwaters including thermal waters.

The proportional coefficients of some of the dissolved components (including ions and gasses) in groundwaters may differ considerably in numerical values in various hydrochemical environments, and recourse to which may be conducive to tracing the cause of groundwater formation. In natural groundwater evolution, Na^+ and Cl^- contents in groundwaters can increase via the intrusion of seawater or the leaching of stratum salt. The mean γNa/γCl coefficient for standard seawater is 0.87 (Li et al., 2006). If the groundwater is mixed with the seawater, the γNa/γCl ratio will approach 0.87, and if the formation salt is extracted into the groundwaters, it will rise to about 1 (Bagheri et al., 2014; Vengosh et al., 1995). In addition, another situation where the ratio is much larger than 1 indicates that the water-rock interaction enhances the exchange between the Ca^{2+} dissolved in the water and the Na^+ adsorbed by the rocks or formations, resulting in the uncoordinated increase of Na^+ and Cl^- concentrations in the waters together with the result of the relatively higher γNa/ γCl ratio. Accordingly, the γNa/γCl value can be used to judge the level of water-rock interaction or cation exchange in groundwaters (Zhou et al., 2015; Wang et al., 2019). The graph of γNa/γCl changing with Cl^- concentration in collected waters of the studied geothermal fields is shown in Fig. 9a. The γNa/γCl from the XZ, SZ, and MM fields were all close to 0.87 except for MM20 (γNa/γCl >1), whereas all water samples from the HZ and FS fields were expressed as γNa/γCl >1, indicating that the coastal seawater had obvious effects on the XZ, SZ, and MM fields, but little on the HZ and FS fields. Also as illustrated in the Gibbs diagram (Gibbs, 1970, 1971), values of TDS and $Cl^-/(Cl^-+HCO_3^-)$ in the HZ and FS fields were both low and HCO_3^- and Na^+ were the main constituents in the geothermal waters possessing the typical characteristics formed under the action of rock weathering and leaching. However, values of TDS and $Cl^-/(Cl^-+HCO_3^-)$ in the coastal areas (XZ, SZ, MM geothermal fields) were both high and samples distributed close to the seawater end-member with dominant ions of Na^+ and Cl^-, especially for the thermal waters of the SZ geothermal field (Fig. 9b). This sharp contrast found in thermal waters between these five geothermal fields proved the pronounced discrimination in the degree of seawater influence.

The dramatic isotope differentiation between the seawater and fresh waters allows a preferable presentation of scenarios with different mixing proportions of seawater in the δ_D-$\delta^{18}O$ relationship diagram (Pang et al., 1990). As shown in Fig. 10a, most of the geothermal waters in the study area were distributed near the global meteoric water line (GMWL) denoting the dominant recharging source of atmospheric precipitation. Besides, samples from the XZ, SZ, and MM fields approached closer to the end member of seawater than those of the other two fields, which elucidated well the distinct mixing degrees of thermal waters with the seawater. Recently, a conservative mixing line between the freshwater and seawater composed of diverse isotope values was constructed to calculate the relative fractional contribution of these two endmembers in the mixed water based on the solute mass balance model, and the mixing ratio (f) can be obtained utilizing a general binary mixing Eq. (2) (Pang et al., 1990; Wang et al., 2018):

$$\delta_m = \delta_s \times f + \delta_f \times (1 - f) \quad (2)$$

where δ_m, δ_s, and δ_f represents the isotope values (δ_D or $\delta^{18}O$) for mixed water, seawater, and fresh groundwater, respectively. f is the fraction of seawater in the mixture. Herein, the isotope values for seawater were referenced by Xu Fang (2016) and were assigned as −23.7‰ (δ_D) and −4‰ ($\delta^{18}O$). From Fig. 10b, it is notable that both δ_D and $\delta^{18}O$ show fairly linear relationships with the concentrations of Cl^-. This means

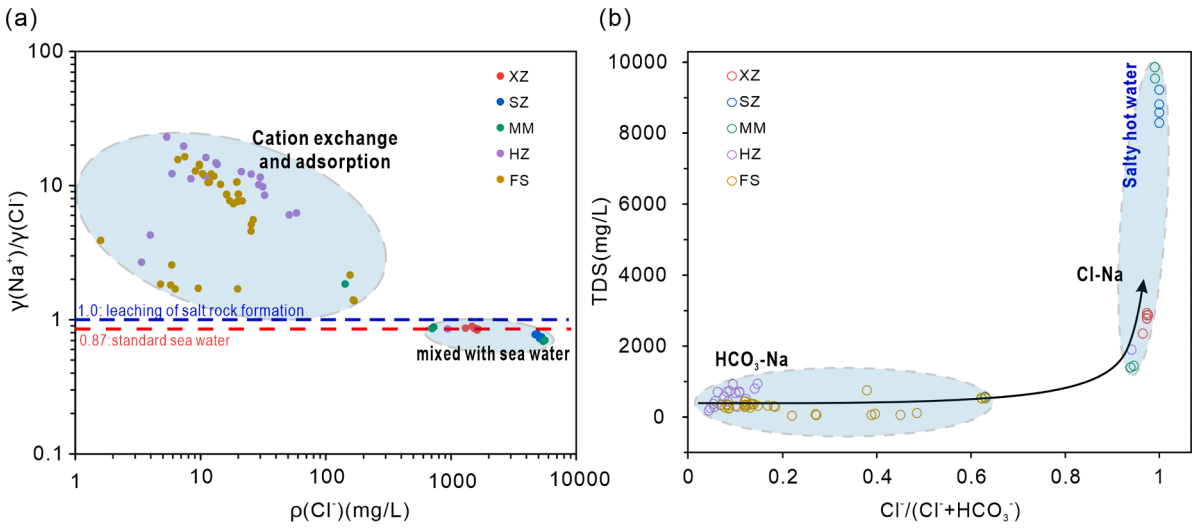

Fig. 9. Plots of the ratio of $\gamma(Na^+)/\gamma(Cl^-)$ vs. the constant of Cl^-, and TDS vs. the ratio of $Cl^-/Cl^-+HCO_3^-$ of waters in the five geothermal fields.

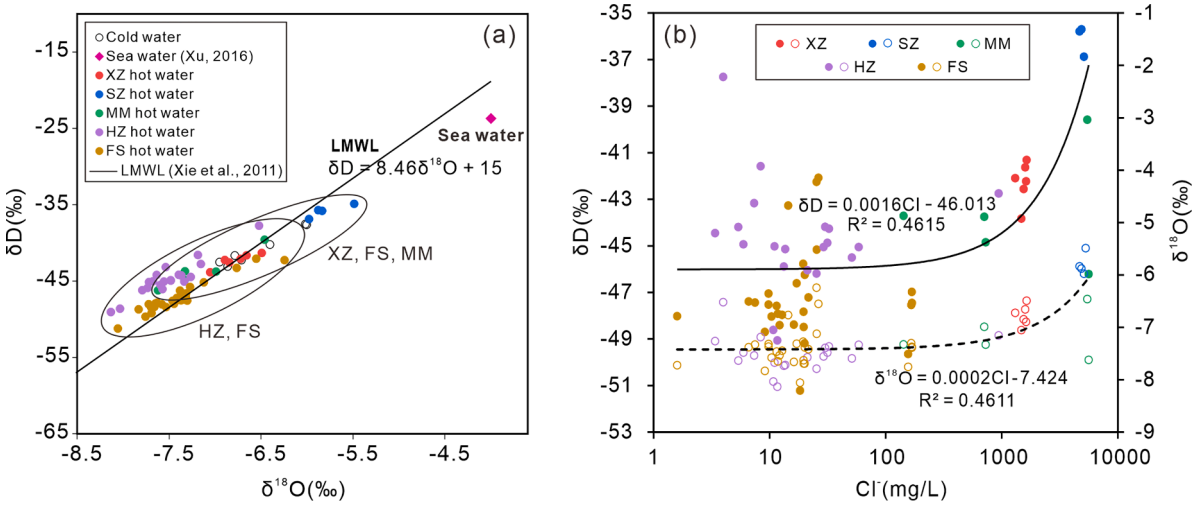

Fig. 10. (a) The local meteoric water line (LMWL) in the study area. (b) The relationships between δ D, $\delta^{18}O$ and content of Cl^- of waters for the five geothermal fields in which the solid and hollow dots represent the results based on δ D and $\delta^{18}O$, respectively.

that the isotope values for thermal waters fluctuate regularly with the continuous intrusion of seawater. Thus, the isotope endmembers of freshwater for δ_D and $\delta^{18}O$ were hypothesized as the isotope values when the concentration of Cl^- was 0 mg/L, and they were ultimately assigned as −46.013‰ and −7.424‰, respectively.

Using this method, the quantitative mixing ratios (*f*) for thermal waters in the five geothermal fields were acquired and the result is listed in Table 3. The calculated *f* based on the δ_D in the XZ and MM areas were proximate and both above 10, and the ratios in the SZ area were the highest overall exceeding 40. However, a somewhat lower range of *f* was achieved in the HZ and FS areas varying between 0.58 to 37.7 with an average of 9.39. The results calculated following the $\delta^{18}O$ showed similarities with that using δ_D. Likewise, Wang et al. (2018) calculated the mixing proportion of seawater in the XZ and SZ geothermal fields by the same approach and concluded that *f* in the SZ geothermal field (39.96–44.33) was higher than that in the XZ geothermal field (12.42–22.05). Through analysis of hydrochemistry of coastal geothermal fields in western Guangdong, Yuan et al. (2013) also found that the local thermal waters were obviously mixed with the modern seawater, and the mixing ratio was between 10.39 and 30.9.

Coupling the results of this study and the present findings substantially illustrates that the geothermal waters of the main geothermal fields like the XZ, SZ and MM in the coastal areas of the Guangdong Province are mostly mixed with seawater, while that of the relatively inland geothermal fields like the HZ and FS are insensitive to this effect.

5.3.2. Potential influence of seawater mixing on REEs concentration and fractionation

As discussed above, it was known that the seawater mixing effect was responsible for the significant variance in the features of water chemistry from different geothermal fields. There is also an urgent need to address whether the seawater intrusion reacts with REEs in local geothermal waters. The seawater mixing primarily affects the geothermal system by altering the hydrochemical environments, and although the mainstream factors like pH, temperature, redox condition and complexation reactions on REEs have been discussed in part 5.1, each separate effect is not expected to influence REEs much as proposed by previous studies. Here, the sharp increase in salinity in geothermal waters caused by seawater intrusion is plausibly suggested to be a pivotal factor accounting for the remarkable differentiation of REEs in various geothermal fields.

Owing to the lack of actual field measurement of salinity, the total dissolved solids (TDS) values were hence chosen as a proxy for characterizing the levels of salinity in thermal waters. Given the TDS value

division, Fig. 11 expresses the existence of two different water types for the study area: the wide varying range and extremely high TDS (564~9861 mg/ L) type with the thermal waters of the XZ, SZ, and MM geothermal fields as representatives and the relatively low TDS (37~1898 mg/ L) type with slight volatility in the HZ and FS geothermal fields. Besides, the ΣREEs concentrations in XZ, SZ, and MM fluids as typical coastal geothermal fields performed a visible linear dependence of TDS value (R^2= 0.4384) supporting well the hypothesis of salinity in controlling the REEs concentrations for offshore thermal waters. However, for the HZ and FS geothermal fields, the extent of ΣREEs shift was large and the ΣREEs seemed not to be associated with the TDS values. This striking contrast illustrated the gradual invalidity for TDS to take effects on REEs concentrations modulation in thermal waters from the ocean to inland.

Generally, REEs do not entirely exist in the free form (Ln^{3+}, Ln represents the REEs) in groundwaters and anions that can complex with REEs mainly include PO_4^{3-} (Lee and Byrne, 1992), hydroxide (OH^-) (Klungness and Byrne 2000; Lee and Byrne, 1992), carbonate (CO_3^{2-}) (Liu and Byrne, 1998; Luo and Byrne, 2004), sulfate (SO_4^{2-}) (Schijf and Byrne,2004), and fluoride (F^-) (Luo and Millero, 2004) essentially depending on the stability constant of the complex reactions between REEs and different ligands, thus the aqueous REEs are diverse in various environments (Haas et al., 1995). Despite the highest complexation stability constant, the phosphate (PO_4^{3-}) was not considered in previous simulations due to its many orders of magnitude lower concentration than many other anions in groundwaters (Johannesson et al., 1995). For the rest anions like nitrate (NO_3^-), and chloride (Cl^-) complex weaker with REEs and hence tend to be ignored as well.

Using the PHREEQC3.3 model technique with the internal LLNL database (Parkhurst and Appelo, 2013), the main aqueous species of REEs in the five geothermal fields were determined (Fig. 12a-c). Considering the extremely low molality of Ln-chloride complexes for most geothermal waters output by the simulation result (see the Table S4 in the Supplementary File), the $LnCl^{2+}$/ $LnCl_2^+$ was not included in the discussion of REEs' inorganic complexation reactions, which was in line with the previous research (Lee and Byrne, 1992; Luo andByrne, 2001; Luo and Millero, 2004; Millero, 1992; Ohta and Kawabe, 2001; Schijf and Byrne, 2004). During modeling, the elements La, Gd and Yb were respectively regarded as the representative of LREEs, MREEs and HREEs, and samples only with explicit measuring results for the total three elements were selected for simulations. Interestingly, a unique result that the dissolved REEs species in thermal waters can be substantially diversified into two types consisting of that in the coastal geothermal fields and the relatively inland fields was obtained, which resembled the classification of the hydrochemistry characterization mentioned above. Except for the sample MM20, the dissolved REEs

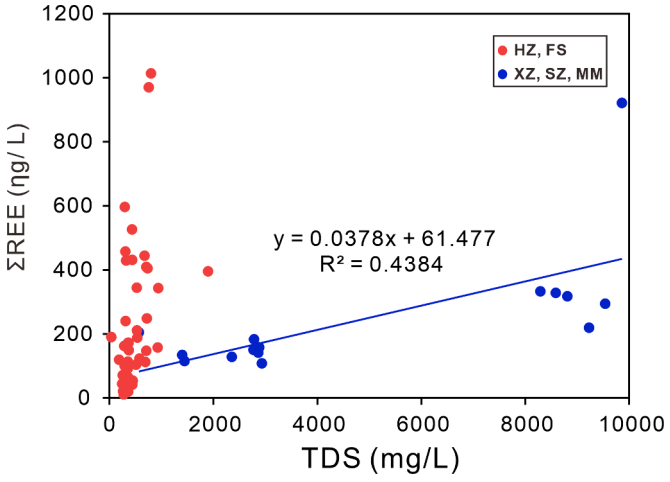

Fig. 11. The relationship between ΣREEs and TDS values in the study area.

existed chiefly in the form of $LnOH^{2+}$ and LnF^{2+} and were less strongly complexed by carbonates and sulfates for the total samples in the XZ, SZ and MM geothermal fields, whereas in the HZ and FS fields, $LnCO_3^+$and Ln $(CO_3)_2^-$ predominated in all thermal waters and other complexing ligands associated with REEs are basically negligible.

To date, numerous investigations have been devoted to studying the mechanism influencing the REE form fractionation observed in groundwaters and pH was proven to be the most critical contributor. It was prevailingly agreed that in neutral to alkaline groundwaters, carbonate complexes were the main species for aqueous REEs (approximately accounting for 70%~100%), manifested as carbonate complexes ($LnCO_3^+$) and dicarbonate complexes (Ln $(CO_3)_2^-$) (Wood, 1990; Zhu et al., 2005; Guo et al., 2010). And the $LnCO_3^+$/ Ln $(CO_3)_2^-$ ratio decreased in step with the increase in pH values, which means that a more alkaline environment facilitated REEs to be complexed with the carbonate-bearing ligands, particularly bicarbonates. However, REE-sulfate ($LnSO_4^+$) took precedence over other species under acid conditions especially for pH less than 6 (Johannesson and Lyons, 1995; Wood, 1990). In addition, after a series of calculations of REE speciation in thermal waters, similar findings emerged. Wang et al. (2020) investigated the species of aqueous REEs in the Tengchong geothermal field as a typically high-temperature geothermal system and concluded that pH determined the mode of occurrence of REEs in local hot waters. Another case recently reported in the Daggyai hydrothermal area with numerous high-temperature hot springs also indicated that the aqueous REEs speciation can be used as a reflection of pH conditions in thermal waters (Guo and Zhang, 2022). The result of REEs speciation calculations conducted by Yuan et al. (2014) realized that REEs transport may be enhanced by the formation of free ions (Ln^{3+}), $LnCO_3^+$ and Ln $(CO_3)_2^-$ when pH at the interval of 5.5~6.5, 6.5~7.5 and greater than 7.5, respectively. Overall, these findings were consistent with those reported in systems of surface water and shallow groundwaters. However, the other forces potentially driving the REEs occurrence mechanism like the temperature and salinity of water were poorly documented. Herein, the physicochemical indices of temperature, pH, ORP and TDS (approximately representing the salinity of local waters) in the study area varying with water samples were all given in the Fig. 12d to ascertain the most contributive factor for REEs' speciation in local thermal waters.

The temperature and ORP both showed a random fluctuation and minor distinction between the two types of waters, which could not decipher the strong differences in the REEs' speciation. Next, the pH values of chosen geothermal water samples varied with a small range between 6.77 and 8.61 belonging to the neutral or weakly alkaline water. If the complexation reactions followed the fluctuation of pH, the REEs' species should not generate such a particularly significant differentiation. Gratifyingly, the TDS values experienced an abrupt reduction from greater than 1 g/L to lower than 1 g/L just in line with the sudden conversion of REEs occurrence modes in thermal waters coincidently from the sample MM20. This adequately emphasized the great importance of TDS (or salinity) in the arrangement of REEs forms in fluids and thus causing the severe differentiation. Fig. 13 showed the proportional changes of main REEs' species with TDS values in the two-type waters. It can be seen that the occurrence patterns of LREEs (represented by La), MREEs (Gd) and HREEs (Yb) varied with TDS values congruently in the same type of water (the type of TDS> 1 g/L (Fig. 13a, c, e) and the type of TDS< 1 g/L (Fig. 13b, d, f)). For thermal waters of TDS> 1 g/L, remarkably positively linear correlations between the proportions of free ions or REE-complexes (including Ln^{3+}, LnF^{2+} and $LnSO_4^+$) and TDS are observed except for the $LnOH^{2+}$ having a negative relationship with TDS. This implied that in a generally salinity-rich hydrothermal fluid, the salinity could make a difference in the amounts of Ln^{3+}, $LnOH^{2+}$, LnF^{2+} and $LnSO_4^+$, and release of free ions (Ln^{3+}) or complexations like fluoride and sulfate with REEs would be strengthened but conversely be inhibited for the formation of $LnOH^{2+}$ along with the growth of salt in water. For thermal waters of TDS< 1 g/L, there were nonlinearly TDS dependent for $LnCO_3^+$ and Ln $(CO_3)_2^-$

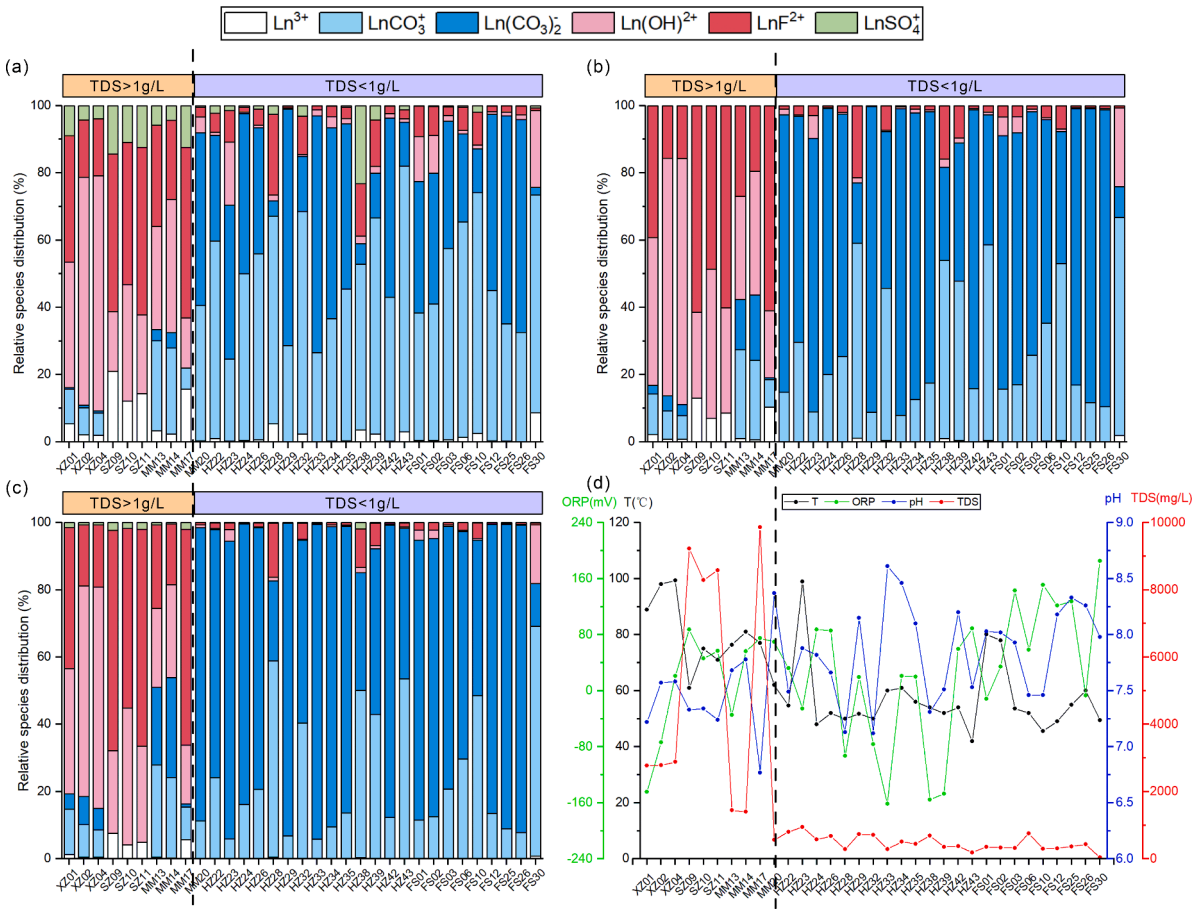

Fig. 12. (a-c) The aqueous REEs' speciation in the five geothermal fields and (a), (b), (c) represent the results for La, Gd, and Yb, respectively. (d) The physico-chemical indices of temperature, pH, ORP, and TDS vary between water samples in the study area.

proportions but an inverting phase change between $LnCO_3^+$ and $Ln(CO_3)_2^-$ appeared as TDS varied. The turning points of $LnCO_3^+$ and $Ln(CO_3)_2^-$ fractions were probably at the TDS of 500 mg/L and 700 mg/L, which determined whether REEs were preferentially bound to one single carbonate or two carbonate ions. When the TDS values were extremely low (high, not exceeding 1 g/L), especially below 300 mg/L (above 900 mg/L), the proportion of $LnCO_3^+$ in thermal waters was always higher than $Ln(CO_3)_2^-$; while complexation with carbonates across the lanthanide series was apparently different when TDS was raised: for the element La as the representative of LREEs (Fig. 13b), the mutual competing processes was a trade-off and comparable between these two species; however, in spite of being characterized as relatively large fluctuations, the $Ln(CO_3)_2^-$ proportion of MREEs (Gd as a representative, Fig. 13d) and HREEs (Yb as a representative, Fig. 13f) was persistently greater than that of $LnCO_3^+$ when TDS was above 300 mg/L. Accordingly, the bicarbonate seemed to be more approachable to REEs with an increasing atomic number when TDS was in the interval of 0.3~ 1 g/L.

In brief, such facts confirm the potentially robust capability for TDS/ salinities modulating the REEs' forms in aqueous systems. However, how salinity affects the species of aqueous REEs in groundwaters still remains a matter of debate. In a particular groundwater environment, the fundamental determinant of REEs-complexes composition is the stable constant of complexing reactions between REEs and diverse ligands (Noack et al., 2014). Studies have noted that temperature (Haas et al., 1995), pressure (Haas et al., 1995), ionic strength (Millero, 1992), and concentration of certain ions (Gosselin et al., 1992; Zhu et al., 2005; Gimeno Serrano et al., 2000) in solution can all alter the stability constants and thus affect the REEs' speciation modes in water bodies. For the most typical example, hyperfluoric acid water was proven to be often associated with high aluminum concentrations so that the inhibition of fluoride complexes by aluminums at low temperatures prevents fluorides from playing an important role in REEs' speciation, whereas under high-temperature conditions, fluoride complexes can be of a great significance due to the increasingly stable property of REE-fluoride in acid water lack of aluminum (Haas et al., 1995; Gimeno Serrano et al., 2000). In our study, another possibility affecting REEs presence was first proposed that the TDS/ salinity of thermal waters was reshaped by a seawater intrusion and indirectly contributed to the fractionation of REEs species appearing in fluids. Certainly, previous experiments have been conducted to determine the concentration changes for partial radioactive REEs at various salinities by mixing filtered seawater and freshwater with different proportions, and it has been suggested that the salinity mutation indeed reacted on the removal of REEs in solution when rivers enter the sea (Elderfield et al., 1990). However, the effects of seawater mixing on the REE concentration of widely collected geothermal waters in the field were hitherto poorly documented and little focused on the research on morphological distribution of aqueous REEs. Herein, it was believed that the salinity/TDS largely affected the occurrence and proportion of dissolved REEs and was speculated to be possibly related to the mechanism of regulating the stability constants of the REE complexation reaction with various ligands. Nevertheless, this was needed to be further confirmed through field sample analyzes and indoor experiments in the future, but an acknowledgement of the salinity/ TDS effect was of a great importance at this stage. This study also provided a new perspective on understanding the occurrence and transport of REEs in coastal geothermal systems.

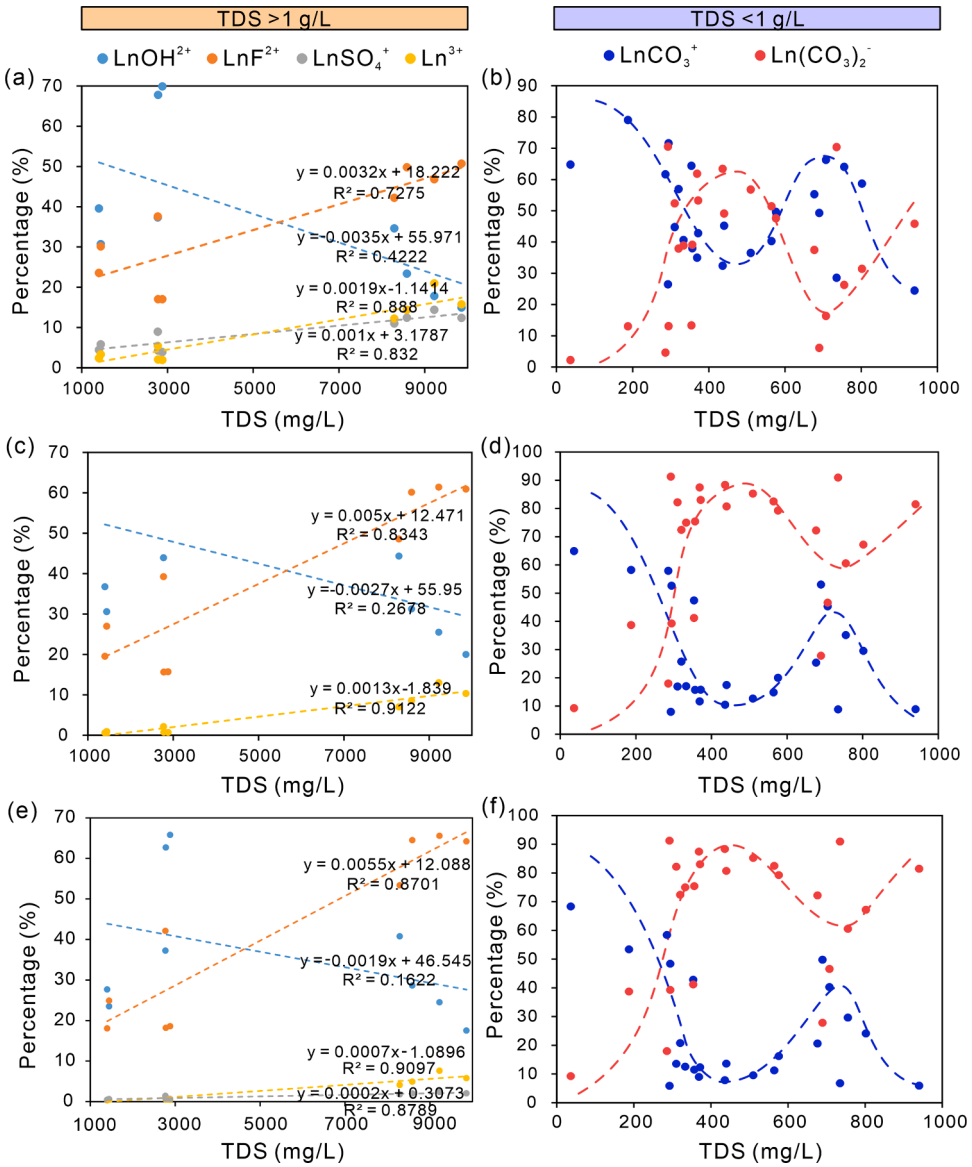

Fig. 13. The proportional changes of REE-complexes with TDS values in two-type waters in which (a), (c), (e) respectively represent the results for the type of TDS >1 g/L and (b), (d), (f) respectively represent the results for the type of TDS <1 g/L. (a) and (b) describe the element of La; (c) and (d) describe the element of Gd; (e) and (f) describe the element of Yb.

6. Conclusion and limitations

Both qualitative and quantitative data results show that thermal water in the studied geothermal fields is widely invaded by seawater, and thermal water in coastal geothermal fields such as Xinzhou, Shenzao, and Maoming is more vulnerable to this effect than that of relatively inland geothermal fields like Huizhou and Fengshun. After normalization by PAAS stand, REEs of geothermal water in the study area present a differentiation mode characterized by the HREE relative enrichment and a significant positive Eu anomaly, and a negative Ce anomaly. The positive Eu anomaly was proved to originate from the preferential dissolution of Eu-rich minerals, especially feldspars constituted most in granites as the major rock type of the local thermal reservoir. The negative Ce anomaly was believed to be due to the seawater mixing effect to an appreciable extent. The REEs concentration in geothermal water was less influenced by pH, temperature, redox conditions, and other environmental factors, whereas it was strongly subject to the water salinity/ TDS values. The transition from coastal areas to inland areas made the positive correlation dependence of the REEs concentration on salinity gradually disappear. Additionally, the speciation of dissolved REEs in geothermal water was also remarkably regulated by water salinity. When TDS> 1 g/ L, REEs mainly exist in the form of Ln^{3+}, $LnOH^{2+}$, $LnSO_4^+$, and LnF^{2+}. Except for $LnOH^{2+}$, other proportions were significantly positively correlated with TDS. However, when TDS< 1 g/ L, $LnCO_3^+$ and Ln $(CO_3)^{2-}$ were dominant and competed with each other. Therefore, in areas with a strong seawater intrusion, the water salinity plays an important role in modulating the concentration and speciation of aqueous REEs. This research emphasizes the great significance of salinity to influence REEs of thermal water, especially in coastal areas. Moreover, it sheds a new light on exploring the occurrence and migration of geothermal REEs in coastal zones.

However, it is just a case study of the influence of salinity on REEs and has not been examined in more depth so far. Additionally, our study is based on the analysis of extensive *in-situ* geothermal water samples, and the occurrence, migration, and transformation of REEs are inherently affected by multiple effects of the surrounding environment. Thus, the internal mechanism it reveals is relatively complicated and how the salinity fluctuation works on the REEs in different geothermal systems

still needs to be verified by more indoor experiments and field sampling and analysis in the future.

CRediT authorship contribution statement

Fen Zhang: Conceptualization, Investigation, Data curation, Formal analysis, Writing – original draft, Writing – review & editing. **Yiman Li:** Funding acquisition, Investigation, Methodology, Validation, Resources, Writing – original draft, Writing – review & editing. **Xiaocheng Zhou:** Funding acquisition, Validation, Resources, Writing – review & editing. **Tianming Huang:** Validation, Resources, Writing – original draft, Writing – review & editing. **Jiao Tian:** Investigation, Writing – review & editing. **Yuanzhi Cheng:** Investigation, Project administration. **Yajing Zhao:** Investigation.

Declaration of Competing Interest

The authors declare that they have no known competing financial interests or personal relationships that could have appeared to influence the work reported in this paper.

Data availability

Data will be made available on request.

Acknowledgements

The study was financially supported by the National Key R&D Program of China (No. 2019YFC0604901), the Key Research Program of the Institute of Geology & Geophysics, CAS (No. IGGCAS-202204), Central Public-interest Scientific Institution Basal Research Fund (CEAIEF20220507, CEAIEF20220213), the National Nature Science Foundation of China (41673106, 42073063, 4193000170, U2039207), and the IGCP Project 724.

Supplementary materials

Supplementary material associated with this article can be found, in the online version, at doi:10.1016/j.geothermics.2023.102826.

References

Awaleh, M.O., Hoch, F.B., Kadieh, I.H., Soubaneh, Y.D., Egueh, N.M., Jalludin, M., Boschetti, T., 2015. The geothermal resources of the Republic of Djibouti — I: hydrogeochemistry of the Obock coastal hot springs. J. Geochem. Explor. 152, 54–66. https://doi.org/10.1016/j.gexplo.2015.02.001.

Bagheri, R., Nadri, A., Raeisi, E., Kazemi, G.A., Eggenkamp, H.G.M., Montaseri, A., 2014. Origin of brine in the Kangan gasfield: isotopic and hydrogeochemical approaches. Environ. Earth Sci. 72 (4), 1055–1072. https://doi.org/10.1007/s12665-013-3022-7.

Banner, J.L., Wasserburg, G.J., Dobson, P.F., Carpenter, A.B., Moore, C.H., 1989. Isotopic and trace element constraints on the origin and evolution of saline groundwaters from central Missouri. Geochim. Cosmochim. Acta 53 (2), 383–398. https://doi.org/10.1016/0016-7037(89)90390-6.

Bau, M., 1991. Rare-earth element mobility during hydrothermal and metamorphic fluid-rock interaction and the significance of the oxidation state of europium. Chem. Geol. 93 (3–4), 219–230. https://doi.org/10.1016/0009-2541(91)90115-8.

Berger, G., Schott, J., Guy, C., 1988. Behavior of Li, Rb and Cs during basalt glass and olivine dissolution and chlorite, smectite and zeolite precipitation from seawater: experimental investigations and modelization between 50° and 300°C. Chem. Geol. 71 (4), 297–312. https://doi.org/10.1016/0009-2541(88)90056-3.

Bragin, I.V., Kharitonova, N.A., Chelnokov, G.A., Aseeva, A.V., Chudaev, O.V., 2018. REY geochemistry in groundwater from Paratunka geothermal area (Kamchatka peninsula, Far East of Russia). Environ. Earth Sci. 77 (10), 376. https://doi.org/10.1007/s12665-018-7571-7.

Brouwer, E., Baeyens, B., Maes, A., Cremers, A., 1983. Cesium and rubidium ion equilibriums in illite clay. J. Phys. Chem. 87 (7), 1213–1219. https://doi.org/10.1021/j100230a024.

Bulia, I.L., Enzweiler, J., 2018. The hydrogeochemistry of bottled mineral water in São Paulo state, Brazil. J. Geochem. Explor. 188, 43–54. https://doi.org/10.1016/j.gexplo.2018.01.007.

Bwire Ojiambo, S., Berry Lyons, W., Welch, K.A., Poreda, R.J., Johannesson, K.H., 2003. Strontium isotopes and rare earth elements as tracers of groundwater–lake water interactions, Lake Naivasha, Kenya. Appl. Geochem. 18 (11), 1789–1805. https://doi.org/10.1016/S0883-2927(03)00104-5.

Cai, S., Lu, J., Huang, Z., Li, R., Li, Z., 2002. Geology of Guangdong Province, Hong Kong and Macao Special Administrative Regions. In: Ma, L. (Ed.), China Geology Atlas. Geological Pubilish House, Beijing.

Cao, J., 2004. Rare earth elements geochemistry of Dongtian gold deposit in western Guangdong. J. Chin. Rare Earth Soc. 22 (2), 275–279.

Censi, P., Mazzola, S., Sprovieri, M., Bonanno, A., Patti, B., Punturo, R., Spoto, S.E., Saiano, F., Alonzo, G., 2004. Rare earth elements distribution in seawater and suspended particulate of the Central Mediterranean Sea. Chem. Ecol. 20, 323–343. https://doi.org/10.1080/02757540410001727954.

Chen, L., Ma, T., Du, Y., Xiao, C., Chen, X., Liu, C., Wang, Y., 2016. Hydrochemical and isotopic (^{2}H, ^{18}O and ^{37}Cl) constraints on evolution of geothermal water in coastal plain of Southwestern Guangdong Province, China. J. Volcanol. Geotherm. Res. 318, 45–54. https://doi.org/10.1016/j.jvolgeores.2016.03.003.

Cholet, C., Steinmann, M., Charlier, J.B., Denimal, S., 2019. Characterizing fluxes of trace metals related to dissolved and suspended matter during a storm event: application to a karst aquifer using trace metals and rare earth elements as provenance indicators. Hydrogeol. J. 27 (1), 305–319. https://doi.org/10.1007/s10040-018-1859-2.

de Baar, H.J.W., German, C.R., Elderfield, H., van Gaans, P., 1988. Rare earth element distributions in anoxic waters of the Cariaco Trench. Geochim. Cosmochim. Acta 52 (5), 1203–1219. https://doi.org/10.1016/0016-7037(88)90275-X.

De Carlo, E.H., Wen, X., Irving, M., 1998. The Influence of redox reactions on the uptake of dissolved Ce by suspended Fe and Mn oxide particles. Aquat. Geochem. 3, 357–389.

Deluca, F., Mongelli, G., Paternoster, M., Zhu, Y., 2020. Rare earth elements distribution and geochemical behaviour in the volcanic groundwaters of Mount Vulture, southern Italy. Chem. Geol. 539, 119503 https://doi.org/10.1016/j.chemgeo.2020.119503.

Deng, Y., Ren, J., Guo, Q., Cao, J., Wang, H., Liu, C., 2017. Rare earth element geochemistry characteristics of seawater and porewater from deep sea in western Pacific. Sci. Rep. 7 (1), 16539. https://doi.org/10.1038/s41598-017-16379-1.

Dia, A., Gruau, G., Olivié-Lauquet, G., Riou, C., Molénat, J., Curmi, P., 2000. The distribution of rare earth elements in groundwaters: assessing the role of source-rock composition, redox changes and colloidal particles. Geochim. Cosmochim. Acta 64 (24), 4131–4151. https://doi.org/10.1016/S0016-7037(00)00494-4.

Dupré, B., Gaillardet, J., Rousseau, D., Allègre, C.J., 1996. Major and trace elements of river-borne material: the Congo Basin. Geochim. Cosmochim. Acta 60 (8), 1301–1321. https://doi.org/10.1016/0016-7037(96)00043-9.

Elderfield, H., Greaves, M.J., 1982. The rare earth elements in seawater. Nature 296 (5854), 214–219. https://doi.org/10.1038/296214a0.

Elderfield, H., Upstill-Goddard, R., Sholkovitz, E.R., 1990. The rare earth elements in rivers, estuaries, and coastal seas and their significance to the composition of ocean waters. Geochim. Cosmochim. Acta 54 (4), 971–991. https://doi.org/10.1016/0016-7037(90)90432-K.

Esmaeili-Vardanjani, M., Shamsipour-Dehkordi, R., Eslami, A., Moosaei, F., Pazand, K., 2013. A study of differentiation pattern and rare earth elements migration in geochemical and hydrogeochemical environments of Airekan and Cheshmeh Shotori areas (Central Iran). Environ. Earth Sci. 68 (3), 719–732. https://doi.org/10.1007/s12665-012-1773-1.

Fee, J.A., Gaudette, H.E., Lyons, W.B., Long, D.T., 1992. Rare-earth element distribution in Lake Tyrrell groundwaters, Victoria, Australia. Chem. Geol. 96 (1–2), 67–93. https://doi.org/10.1016/0009-2541(92)90122-L.

Geological Survey of Guangdong Province, 1988. Regional Geology of Guangdong Province, People's Republic of China. Geology Publishing House, Beijing. Chinese.

Gibbs, R., 1970. Mechanism controlling world river water chemistry. Science 170 (3962), 1088–1090. https://doi.org/10.1126/science.170.3962.1088.

Gibbs, R., 1971. Mechanism controlling world river water chemistry: evaporation-crystallization process. Science 172 (3985), 871–872. https://doi.org/10.1126/science.172.3985.870.

Gimeno Serrano, M.J., Auqué Sanz, L.F., Nordstrom, D.K, 2000. REE speciation in low-temperature acidic waters and the competitive effects of aluminum. Chem. Geol. 165 (3–4), 167–180. https://doi.org/10.1016/S0009-2541(99)00166-7.

Gleason, J.D., Marikos, M.A., Barton, M.D., Johnson, D.A., 2000. Neodymium isotopic study of rare earth element sources and mobility in hydrothermal Fe oxide (Fe-P-REE) systems. Geochim. Cosmochim. Acta 64 (6), 1059–1068. https://doi.org/10.1016/S0016-7037(99)00325-7.

Göb, S., Loges, A., Nolde, N., Bau, M., Jacob, D.E., Markl, G., 2013. Major and trace element compositions (including REE) of mineral, thermal, mine and surface waters in SW Germany and implications for water–rock interaction. Appl. Geochem. 33, 127–152. https://doi.org/10.1016/j.apgeochem.2013.02.006.

Gosselin, D.C., Smith, M.R., Lepel, E.A., Laul, J.C., 1992. Rare earth elements in chloride-rich groundwater, Palo Duro Basin, Texas, USA. Geochim. Cosmochim. Acta 56 (4), 1495–1505. https://doi.org/10.1016/0016-7037(92)90219-9.

Gruau, G., Dia, A., Olivié-Lauquet, G., Davranche, M., Pinay, G., 2004. Controls on the distribution of rare earth elements in shallow groundwaters. Water Res. 38 (16), 3576–3586. https://doi.org/10.1016/j.watres.2004.04.056.

Guo, H., Zhang, B., Wang, G., Shen, Z., 2010. Geochemical controls on arsenic and rare earth elements approximately along a groundwater flow path in the shallow aquifer of the Hetao Basin, Inner Mongolia. Chem. Geol. 270 (1–4), 117–125. https://doi.org/10.1016/j.chemgeo.2009.11.010.

Guo, Q., 2018. Doctoral dissertation. University of Chinese Academy of Sciences, Beijing.

Guo, Q., Zhang, X., 2022. Geochemical behavior of rare earth elements in high-temperature hot springs and its indications: a case study in the Daggyai hydrothermal area, Tibet. Bull. Geological Sci. Technol. 41 (5), 172–180.
Haas, J.R., Shock, E.L., Sassani, D.C., 1995. Rare earth elements in hydrothermal systems: estimates of standard partial molal thermodynamic properties of aqueous complexes of the rare earth elements at high pressures and temperatures. Geochim. Cosmochim. Acta 59, 4329–4350. https://doi.org/10.1016/0016-7037(95)00314-P.
Han, G., Yang, K., Zeng, J., 2021. Distribution and fractionation of rare earth elements in suspended sediment of the Zhujiang River, Southwest China. J. Soils Sediments 21 (8), 2981–2993. https://doi.org/10.1007/s11368-021-03008-8.
Hart, S.R., 1969. K, Rb, Cs contents and K/Rb, K/Cs ratios of fresh and altered submarine basalts. Earth Planet. Sci. Lett. 6 (4), 295–303. https://doi.org/10.1016/0012-821X(69)90171-X.
Hatipoğlu Temizel, E., Gültekin, F., Fırat Ersoy, A., 2020. Major, trace, and rare earth element geochemistry of the Ayder and İkizdere (Rize, NE Turkey) geothermal waters: constraints for water–rock interactions. Geothermics 86, 101810. https://doi.org/10.1016/j.geothermics.2020.101810.
He, S.X., Liu, X.C., Yang, L., Wang, J.M., Hu, F.Y., Wu, F.Y., 2021. Multistage magmatism recorded in a single gneiss dome: insights from the Lhagoi Kangri leucogranites, Himalayan orogen. Lithos 106222, 398–399. https://doi.org/10.1016/j.lithos.2021.106222.
Hetherington, C.J., Harlov, D.E., Budzyń, B., 2010. Experimental metasomatism of monazite and xenotime: mineral stability, REE mobility and fluid composition. Mineral. Petrol. 99 (3–4), 165–184. https://doi.org/10.1007/s00710-010-0110-1.
Huang, Y., Chu, M., 1995. On the relations between the features of geological formation and the geomorphic growth in Guang Dong Province. Yunnan Geograp. Environ. Res. 7 (2), 85–89.
Ingri, J., Widerlund, A., Land, M., Gustafsson, Ö., Andersson, P., Öhlander, B., 2000. Temporal variations in the fractionation of the rare earth elements in a boreal river; the role of colloidal particles. Chem. Geol. 166 (1–2), 23–45. https://doi.org/10.1016/S0009-2541(99)00178-3.
Johannesson, K.H., Farnham, I.M., Guo, C., Stetzenbach, K.J., 1999. Rare earth element fractionation and concentration variations along a groundwater flow path within a shallow, basin-fill aquifer, southern Nevada, USA. Geochim. Cosmochim. Acta 63 (18), 2697–2708. https://doi.org/10.1016/S0016-7037(99)00184-2.
Johannesson, K.H., Lyons, W.B., 1995. Rare-earth element geochemistry of Colour Lake, an acidic freshwater lake on Axel Heiberg Island, Northwest Territories, Canada. Chem. Geol. 119 (1), 209–223. https://doi.org/10.1016/0009-2541(94)00099-T.
Johannesson, K.H., Lyons, W.B., Stetzenbach, K.J., Byrne, R.H., 1995. The solubility control of rare earth elements in natural terrestrial waters and the significance of PO_4^{3-} and CO_3^{2-} in limiting dissolved rare earth concentrations: a review of recent information. Aquat. Geochem. 1 (2), 157–173. https://doi.org/10.1007/BF00702889.
Johannesson, K.H., Stetzenbach, K.J., Hodge, V.F., 1997. Rare earth elements as geochemical tracers of regional groundwater mixing. Geochim. Cosmochim. Acta 61 (17), 3605–3618. https://doi.org/10.1016/S0016-7037(97)00177-4.
Keasler, K.M., Loveland, W.D., 1982. Rare earth elemental concentrations in some Pacific Northwest rivers. Earth Planet. Sci. Lett. 61 (1), 68–72. https://doi.org/10.1016/0012-821X(82)90039-5.
Kizler, C., 2011. Doctoral dissertation, Diploma thesis. Eberhard Karls Universität Tübingen, Germany.
Klungness, G.D., Byrne, R.H., 2000. Comparative hydrolysis behavior of the rare earths and yttrium: the influence of temperature and ionic strength. Polyhedron 19 (1), 99–107. https://doi.org/10.1016/S0277-5387(99)00332-0.
Larsen, W., Liu, X.M., Riveros-Iregui, D.A., 2021. Rare earth element behavior in springs and streams on a basaltic island: San Cristóbal, Galápagos. Appl. Geochem. 131, 105004 https://doi.org/10.1016/j.apgeochem.2021.105004.
Laveuf, C., Cornu, S., 2009. A review on the potentiality of Rare Earth Elements to trace pedogenetic processes. Geoderma 154 (1–2), 1–12. https://doi.org/10.1016/j.geoderma.2009.10.002.
Lee, J.H., Byrne, R.H., 1992. Examination of comparative rare earth element complexation behavior using linear free-energy relationships. Geochim. Cosmochim. Acta 56, 1127–1137. https://doi.org/10.1016/0016-7037(92)90050-S.
Lee, S.G., Lee, D.H., Kim, Y., Chae, B.G., Kim, W.Y., Woo, N.C., 2003. Rare earth elements as indicators of groundwater environment changes in a fractured rock system: evidence from fracture-filling calcite. Appl. Geochem. 18 (1), 135–143. https://doi.org/10.1016/S0883-2927(02)00071-9.
Li, B., Kong, Q., Wang, G., Liu, F., Guo, L., Liu, C., et al., 2022a. Controls on the behaviors of rare earth elements in acidic and alkaline thermal springs. Appl. Geochem. 143, 105379 https://doi.org/10.1016/j.apgeochem.2022.105379.
Li, D., 2005. Present situation and development prospect of geothermal resources in Guangdong Province. In: Proceedings of the National Academic Symposium on Sustainable Development of Geothermal Industry. Chemical Industry Press, pp. 101–107. Chinese.
Li, J., Du, J., Chang, Q., Liu, L., Cui, Y., Xie, C., Sun, Y., 2013. REE concentrations of garnet and omphacite in eclogites from the Dabie Mountain, central China. Chin. J. Geochem. 32 (1), 85–94. https://doi.org/10.1007/s11631-013-0610-x.
Li, T., Tan, H., Fan, Q., 2006. Hydrochemical characteristics and origin analysis of the underground brings in west Qaidam Basin. J. Salt Lake Res. 14 (4), 26–32. https://doi.org/10.3969/j.issn.1008-858X.2006.04.005.
Li, Y., Chen, K., Tian, J., Cheng, Y., Luo, J., Pang, Z., 2022b. REE characteristics and their influencing factors of the geothermal water in Tangkeng geothermal field, Fengshun, Guangdong Province. Geologic. Rev. 68 (3), 993–1005. https://doi.org/10.16509/j.georeview.2022.03.105.
Li, Y., Tian, J., Cheng, Y., Jiang, G., Zhang, Y., Chen, K., Pang, Z., 2021. Existence of high temperature geothermal resources in the igneous rock regions of South China. Front. Earth Sci. 9, 728162 https://doi.org/10.3389/feart.2021.728162.
Liao, Z., 2012. Promoting the development and utilization of medium and low temperature convection geothermal resources. Sci. Technol. Rev. 30 (32), 80.–80Chinese.
Lin, Y., Gao, L., Li, S., Wang, Z., Ye, Z., Chen, J., Yang, Z., 2020. Hydrogeochemical characteristics and source identification of geothermal waters in Jiangmen, Guangdong Province. Environ. Chem. 39 (2), 512–523. Chinese.
Ling, H., Shen, W., Sun, T., Jiang, S., Ni, P., Gao, J., Huang, G., Ye, H., Tan, Z., 2006. Genesis and source characteristics of 22 Yanshanian granites in Guangdong province: study of element and Nd–Sr isotopes. Acta Petrologica Sinica 22 (11), 2687–2703. https://doi.org/10.3321/j.issn:1000-0569.2006.11.007.
Liu, H., Guo, H., Xing, L., Zhan, Y., Li, F., Shao, J., et al., 2016. Geochemical behaviors of rare earth elements in groundwater along a flow path in the North China Plain. J. Asian Earth Sci. 117, 33–51. https://doi.org/10.1016/j.jseaes.2015.11.021.
Liu, H., Pourret, O., Guo, H., Bonhoure, J., 2017. Rare earth elements sorption to iron oxyhydroxide: model development and application to groundwater. Appl. Geochem. 87, 158–166. https://doi.org/10.1016/j.apgeochem.2017.10.020.
Liu, X., Byrne, R.H., 1998. Comprehensive investigation of yttrium and rare earth element complexation by carbonate ions using ICP-mass spectrometry. J. Solution Chem. 27 (9), 803–815. https://doi.org/10.1023/A:1022677119835.
Loges, A., Wagner, T., Barth, M., Bau, M., 2012. Negative Ce anomalies in Mn oxides: the role of Ce^{4+} mobility during water–mineral interaction. Geochim. Cosmochim. Acta 86, 296–317. https://doi.org/10.1016/j.gca.2012.03.017.
Lu, G., Liu, R., 2015. Aqueous chemistry of typical geothermal springs with deep faults in Xinyi and Fengshun in Guangdong Province, China. J. Earth Sci. 26 (1), 60–72. https://doi.org/10.1007/s12583-015-0498-y.
Luo, J., Li, Y., Tian, J., Cheng, Y., Pang, Z., Gong, Y., 2022. Geochemistry of geothermal fluid with implications on circulation and evolution in Fengshun-Tangkeng geothermal field, South China. Geothermics 100, 102323. https://doi.org/10.1016/j.geothermics.2021.102323.
Luo, Y., Millero, F.J., 2004. Effects of temperature and ionic strength on the stabilities of the first and second fluoride complexes of yttrium and the rare earth elements. Geochim. Cosmochim. Acta 68 (21), 4301–4308. https://doi.org/10.1016/j.gca.2004.05.025.
Luo, Y.R., Byrne, R.H., 2001. Yttrium and rare earth element complexation by chloride ions at 25 °C. J. Solution Chem. 30 (9), 837–845. https://doi.org/10.1023/A:1012292417793.
Luo, Y.R., Byrne, R.H., 2004. Carbonate complexation of yttrium and the rare earth elements in natural waters. Geochim. Cosmochim. Acta 68 (4), 691–699. https://doi.org/10.1016/S0016-7037(03)00495-2.
Ma, L., Dang, D., Wang, W., Evans, R.D., Wang, W., 2019. Rare earth elements in the Pearl River Delta of China: potential impacts of the REE industry on water, suspended particles and oysters. Environ. Pollut. 244, 190–201. https://doi.org/10.1016/j.envpol.2018.10.015.
Mao, X., Wang, H., Feng, L., 2018. Impact of additional dead carbon on the circulation estimation of thermal springs exposed from deep-seated faults in the Dongguan basin, southern China. J. Volcanol. Geotherm. Res. 361, 1–11. https://doi.org/10.1016/j.jvolgeores.2018.08.002.
Mao, X., Wang, Y., Zhan, H., Feng, L., 2015. Geochemical and isotopic characteristics of geothermal springs hosted by deep-seated faults in Dongguan Basin, Southern China. J. Geochem. Explor. 158, 112–121. https://doi.org/10.1016/j.gexplo.2015.07.008.
McLennan, S., 2018. Chapter 7. Rare earth elements in sedimentary rocks: influence of provenance and sedimentary processes. In: Lipin, B., McKay, G. (Eds.), Geochemistry and Mineralogy of Rare Earth Elements. De Gruyter, Berlin, Boston, pp. 169–200. https://doi.org/10.1515/9781501509032-010.
Ménard, O., Advocat, T., Ambrosi, J.P., Michard, A., 1998. Behaviour of actinides (Th, U, Np and Pu) and rare earths (La, Ce and Nd) during aqueous leaching of a nuclear glass under geological disposal conditions. Appl. Geochem. 13 (1), 105–126. https://doi.org/10.1016/S0883-2927(97)00057-7.
Miekeley, N., de Jesus, H.C., da Silveira, C.L.P., Linsalata, P., Morse, R., 1992. Rare-earth elements in groundwaters from the Osamu Utsumi mine and Morro do Ferro analogue study sites, Poços de Caldas, Brazil. J. Geochem. Explor. 45, 365–387. https://doi.org/10.1016/0375-6742(92)90131-Q.
Millero, F.J., 1992. Stability constants for the formation of rare earth-inorganic complexes as a function of ionic strength. Geochemica et Cosmochimica Acta 56, 3123–3132. https://doi.org/10.1016/0016-7037(92)90293-R.
Motoki, A., Sichel, S.E., Vargas, T., Melo, D.P., Motoki, K.F., 2015. Geochemical behaviour of trace elements during fractional crystallization and crustal assimilation of the felsic alkaline magmas of the state of Rio de Janeiro, Brazil. Anais Da Academia Brasileira de Ciências 87 (4), 1959–1979. https://doi.org/10.1590/0001-3765201520130385.
Murray, R.W., Buchholtz ten Brink, M.R., Jones, D.L., Gerlach, D.C., Russ III, G.P., 1990. Rare earth elements as indicators of different marine depositional environments in chert and shale. Geology 18 (3), 268–271. https://doi.org/10.1130/0091-7613(1990)018<0268:REEAIO>2.3.CO;2.
Muzaffer Karadağ, M., Küpeli, Ş., Arýk, F., Ayhan, A., Zedef, V., Döyen, A., 2009. Rare earth element (REE) geochemistry and genetic implications of the Mortaş bauxite deposit (Seydişehir/Konya – Southern Turkey). Geochemistry 69 (2), 143–159. https://doi.org/10.1016/j.chemer.2008.04.005.
Nelson, B.J., Wood, S.A., Osiensky, J.L., 2003. Partitioning of REE between solution and particulate matter in natural waters: a filtration study. J. Solid State Chem. 171 (1–2), 51–56. https://doi.org/10.1016/S0022-4596(02)00145-7.

Noack, C.W., Dzombak, D.A., Karamalidis, A.K., 2014. Rare earth element distributions and trends in natural waters with a focus on groundwater. Environ. Sci. Technol. 48 (8), 4317–4326. https://doi.org/10.1021/es4053895.

Ohta, A., Kawabe, I., 2001. REE(III) adsorption onto Mn dioxide (δ-MnO_2) and Fe oxyhydroxide: ce (III) oxidation by δ-MnO_2. Geochim. Cosmochim. Acta 65 (5), 695–703. https://doi.org/10.1016/S0016-7037(00)00578-0.

Oliveri, Y., Cangemi, M., Capasso, G., Saiano, F., 2019. Pathways and fate of REE in the shallow hydrothermal aquifer of Vulcano island (Italy). Chem. Geol. 512, 121–129. https://doi.org/10.1016/j.chemgeo.2019.02.037.

Pang, Z., Fan, Z., Wang, J., 1990. The study on stable oxygen and hydrogen isotopes in the Zhangzhou Basin hydrothermal system. Acta Petrologica Sinica 6 (4), 75–84.

Parkhurst, D.L., Appelo, C.A.J., 2013. Description of Input and Examples For PHREEQC Version 3—A Computer Program For speciation, batch-reaction, One-Dimensional transport, and Inverse Geochemical calculations: U.S. Geological Survey Techniques and Methods, Book 6, chap. A43, p. 497 pavailable only at. https://pubs.usgs.gov/tm/06/a43/.

Pourret, O., Davranche, M., Gruau, G., Dia, A., 2007. Organic complexation of rare earth elements in natural waters: evaluating model calculations from ultrafiltration data. Geochim. Cosmochim. Acta 71 (11), 2718–2735. https://doi.org/10.1016/j.gca.2007.04.001.

Pourret, O., Gruau, G., Dia, A., Davranche, M., Molénat, J., 2010. Colloidal control on the distribution of rare earth elements in shallow groundwaters. Aquat. Geochem. 16 (1), 31–59. https://doi.org/10.1007/s10498-009-9069-0.

Schijf, J., Byrne, R.H., 2004. Determination of $_{SO4}\beta 1$ for yttrium and the rare earth elements at I = 0.66m and t = 25°C—Implications for YREE solution speciation in sulfate-rich waters. Geochim. Cosmochim. Acta 68 (13), 2825–2837. https://doi.org/10.1016/j.gca.2003.12.003.

Shakeri, A., Ghoreyshinia, S., Mehrabi, B., Delavari, M., 2015. Rare earth elements geochemistry in springs from Taftan geothermal area SE Iran. J. Volcanol. Geotherm. Res. 304, 49–61. https://doi.org/10.1016/j.jvolgeores.2015.07.023.

Sholkovitz, E.R., 1992. Chemical evolution of rare earth elements: fractionation between colloidal and solution phases of filtered river water. Earth Planet. Sci. Lett. 114 (1), 77–84. https://doi.org/10.1016/0012-821X(92)90152-L.

Smedley, P.L., 1991. The geochemistry of rare earth elements in groundwater from the Carnmenellis area, southwest England. Geochim. Cosmochim. Acta 55, 2767–2779.

Stern, J.C., Sonke, J.E., Salters, V.J.M., 2007. A capillary electrophoresis-ICP-MS study of rare earth element complexation by humic acids. Chem. Geol. 246 (3–4), 170–180. https://doi.org/10.1016/j.chemgeo.2007.09.008.

Sverjensky, D.A., 1984. Europium redox equilibria in aqueous solution. Earth Planet. Sci. Lett. 67 (1), 70–78. https://doi.org/10.1016/0012-821X(84)90039-6.

Tian, J., Li, Y., Zhou, X., Pang, Z., Li, L., Xing, L., Li, Z., 2021. Geochemical characteristics of hydrothermal volatiles from Southeast China and their implications on the tectonic structure controlling heat convection. Front. Earth Sci. 9, 786051 https://doi.org/10.3389/feart.2021.786051.

Vengosh, A., Chivas, A.R., Starinsky, A., Kolodny, Y., Baozhen, Z., Pengxi, Z., 1995. Chemical and boron isotope compositions of non-marine brines from the Qaidam Basin, Qinghai, China. Chem. Geol. 120 (1–2), 135–154. https://doi.org/10.1016/0009-2541(94)00118-R.

Verplanck, P.L., Nordstrom, D.K., Taylor, H.E., Kimball, B.A., 2004. Rare earth element partitioning between hydrous ferric oxides and acid mine water during iron oxidation. Appl. Geochem. 19 (8), 1339–1354. https://doi.org/10.1016/j.apgeochem.2004.01.016.

Wampler, J.M., Krogstad, E.J., Elliott, W.C., Kahn, B., Kaplan, D.I., 2012. Long-term selective retention of natural Cs and Rb by highly weathered coastal plain soils. Environ. Sci. Technol. 46 (7), 3837–3843. https://doi.org/10.1021/es2035834.

Wang, B., Lu, G., Hu, X., Ou, H., 2019. Hydrochemical characterization of thermal spring waters in the deep fault region in western Guangdong. Environ. Chem. 38 (5), 1150–1160. https://doi.org/10.7524/j.issn.0254-6108.2018101803.

Wang, M., Zhou, X., Liu, Y., Xu, H., Wu, Y., Zhuo, L., 2020. Major, trace and rare earth elements geochemistry of geothermal waters from the Rehai high-temperature geothermal field in Tengchong of China. Appl. Geochem. 119, 104639 https://doi.org/10.1016/j.apgeochem.2020.104639.

Wang, X., 2008. Doctoral dissertation. China University of Geosciences, Wuhan.

Wang, X., Lu, G., Hu, B.X., 2018. Hydrogeochemical characteristics and geothermometry applications of thermal waters in coastal xinzhou and shenzao geothermal Fields, Guangdong, China. Geofluids 2018, 1–24. https://doi.org/10.1155/2018/8715080.

Wood, S.A., 1990. The aqueous geochemistry of the rare earth elements and yttrium. Part I. Review of available low temperature data for inorganic complexes and the inorganic REE speciation of natural waters. Chem. Geol. 82, 159–186. https://doi.org/10.1016/0009-2541(90)90080-Q.

Wu, M., Cheng, H., Qin, X., 2020. Analysis on distribution and occurrence characteristics of geothermal resources in Huizhou City. Western Resour. (4), 137–139. https://doi.org/10.16631/j.cnki.cn15-1331/p.2020.04.049.

Wu, M., Li, X., Liu, Y., Wei, K., 2003. Rare earth elements in groundwaters from Fogang granitoid weathering crust of Baisha, Yingde, Guangdong Province, China. Geochimica 32 (4), 335–342.

Xiao, C., Wang, Q., Zhou, X., Yang, L., Zhang, J., 2010. Rare-earth elements in hot spring waters in the Tengchong geothermal area. Acta Petrologica Sinica 26 (6), 1938–1944.

Xu Fang, Y., 2016. Master's thesis. China University of Geosciences, Wuhan.

Yan, X., Gan, H., Yue, G., 2019. Hydrogeochemical characteristics and genesis of typical geothermal fileds from Huangshadong to Conghua in Guangdong. Geologic. Rev. 65 (3), 743–754. https://doi.org/10.16509/j.georeview.2019.03.018.

Yuan, J., Mao, X., Wang, Y., 2013. Hydrogeochemical characteristics of low to medium temperature groundwater in the Pearl River Delta Region, China. Procedia Earth Planetary Sci. 7, 928–931. https://doi.org/10.1016/j.proeps.2013.03.179.

Yuan, J., Mao, X., Wang, Y., Deng, Z., Huang, L., 2014. Geochemistry of rare-earth elements in shallow groundwater, northeastern Guangdong Province, China. Chin. J. Geochem. 33 (1), 53–64. https://doi.org/10.1007/s11631-014-0659-1.

Zhou, H., Tan, H., Gao, J., Zhang, W., 2015. Analysis of salinization mechanism of groundwater in Nantong area and its improvement measures. Water Resour. Protect. 31 (4), 70–76. https://doi.org/10.3880/j.issn.1004-6933.2015.04.013.

Zhu, C., 1982. Control of fault structure on geothermal water in Guangdong province. Hydrogeol. Eng. Geol. (06), 17–41. Chinese.

Zhu, X., 2017. Doctoral dissertation. Xiamen University.

Zhu, Z., Liu, C., Wang, Z., Li, J., Zhou, Z., 2005. Inorganic speciation of rare earth elements in Chaohu Lake and Longganhu Lake, East China. J. Rare Earths 23 (6), 768–772.